NASA TECHNICAL NOTE

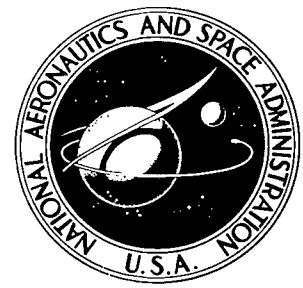

NASA TN D-8181

NASA TN D-8181

LOAN COPY: RETI
AFWL TECHNICAL I
KIRTLAND AFB,

THEORY OF LOW TRANSITIONS IN CO DISCHARGE LASERS

Barry D. Sidney, Roy M. McInville, Neill S. Smith, and H. A. Hassan

Langley Research Center
Hampton, Va. 23665

NATIONAL AERONAUTICS AND SPACE ADMINISTRATION • WASHINGTON, D. C. • MAY 1976

TECH LIBRARY KAFB, NM
0133844

1. Report No.	2. Government Accession No.	3. Recipient's
NASA TN D-8181		

4. Title and Subtitle

THEORY OF LOW TRANSITIONS IN CO DISCHARGE LASERS

5. Report Date: May 1976

6. Performing Organization Code

7. Author(s)

Barry D. Sidney, Roy M. McInville, Neill S. Smith, and H. A. Hassan

8. Performing Organization Report No.: L-10589

10. Work Unit No.: 506-25-43-01

9. Performing Organization Name and Address

NASA Langley Research Center
Hampton, Va. 23665

11. Contract or Grant No.

13. Type of Report and Period Covered: Technical Note

12. Sponsoring Agency Name and Address

National Aeronautics and Space Administration
Washington, D.C. 20546

14. Sponsoring Agency Code

15. Supplementary Notes

Barry D. Sidney: Langley Research Center.
Roy M. McInville, Neill S. Smith, and H. A. Hassan: North Carolina State University at Raleigh.

16. Abstract

A self-consistent theoretical model which couples the electron and heavy particle finite-rate kinetics with the optical and fluid dynamic processes has been employed to identify the various parameters and explain the mechanism responsible for producing low-lying transitions in slow-flowing CO lasers. It is found that lasing on low-lying transitions can be achieved at low temperatures for low pressures (or low-flow rates) together with high partial pressures of He and N_2. The role of N_2 has been identified as an additive responsible for reducing the electron temperature to a range where the transfer of electrical power to the lower vibrational modes of CO is optimum.

17. Key Words (Suggested by Author(s))

CO laser
Chemical kinetics

18. Distribution Statement

Unclassified – Unlimited

Subject Category 36

19. Security Classif. (of this report)	20. Security Classif. (of this page)	21. No. of Pages	22. Price*
Unclassified	Unclassified	68	$4.25

*For sale by the National Technical Information Service, Springfield, Virginia 22161

THEORY OF LOW TRANSITIONS IN CO DISCHARGE LASERS

Barry D. Sidney, Roy M. McInville,* Neill S. Smith,*
and H. A. Hassan*
Langley Research Center

SUMMARY

A self-consistent theoretical model which couples the electron and heavy particle finite-rate kinetics with the optical and fluid dynamic processes has been employed to identify the various parameters and explain the mechanism responsible for producing low-lying transitions in slow-flowing CO lasers. It is found that lasing on low-lying transitions can be achieved at low temperatures for low pressures (or low-flow rates) together with high partial pressures of He and N_2. The role of N_2 has been identified as an additive responsible for reducing the electron temperature to a range where the transfer of electrical power to the lower vibrational modes of CO is optimum.

INTRODUCTION

Molecular gas lasers have received considerable attention in recent years because of their high efficiencies and high power capabilities in the infrared region. The CO laser is of particular interest because of its high quantum efficiency and its ability to oscillate on a number of vibrational-rotational bands. Transitions involving higher vibrational bands are strongly attenuated by atmospheric water vapor; however, low-lying transitions with wavelengths below 5 μm propagate in the atmosphere with relatively high transmittivity. (See ref. 1.) Moreover, the $1 \rightarrow 0$ transition can be used for detecting CO in long-path absorption measurements. Thus, the ability of the CO laser to operate on low-lying vibrational bands in the 5-μm region makes it an indispensable tool in atmospheric transmission and probing experiments.

The objective of this study is to identify the various parameters and explain the mechanism responsible for producing low-lying vibrational transitions in CO laser systems. Experiments (refs. 2 to 4) have shown that low temperature and low CO concentration in a CO-N_2-He electric discharge system are two factors influencing the appearance of low-lying vibrational transitions. Both of these effects were evident in the recent analysis of the high-flow laser systems by Smith and Hassan. (See ref. 5.)

---

*North Carolina State University at Raleigh.

For the study reported in this paper, a self-consistent model was formulated and was used to evaluate the manner in which the operating conditions, that is, pressure, flow rate, mixture ratios and power, affect the low-lying transitions. The need for a self-consistent model became evident because earlier analyses of slow-flow CO lasers (refs. 2 and 6 to 8) assumed certain flow properties which could be determined as part of the solution. Thus, the theories of references 2, 6, and 7 assume the electron distribution function to be Maxwellian at some given electron temperature; moreover, these theories assume the electron number density and the gas temperature. The effect of such assumptions is that important phenomena resulting from the coupling of the kinetics and fluid dynamic processes of the electrons and heavy particles are ignored. Center and Caledonia (ref. 8) have also presented calculations for slow-flow CO lasers in which the distribution function was obtained from a solution of an appropriate Boltzmann equation; however, they had to assume a value for the gas temperature. In contrast to these theories, the present model couples the kinetics of the electrons and heavy particles with the optical and fluid dynamic processes in the laser system. It treats molecules in different quantum states as different species and employs the electron Boltzmann equation and the conservation of species, mass, momentum, and energy equations to describe the system. For a given geometry, voltage, current, gas composition, pressure, mass flow rate, and reflectivities, the theory can predict the number densities of the electrons and the excited states of the heavy particles, the electron and gas temperatures, the intensities of the lasing transitions, and efficiency.

These theoretical results are compared with gain and intensity measurements obtained with a slow-flow CO electric discharge laser of conventional design. (See ref. 9 and fig. 1.) In general, the comparisons show good agreement and indicate the validity of the model developed here.

The work carried out at North Carolina State University at Raleigh was supported in part by NASA Grant NSG-1013.

SYMBOLS

A	cross-sectional area of laser tube
A_{st}	empirical constant in equation (A20)
$A(u)$	quantity defined by equations (B7)
$A_v^{(1)}, A_v^{(2)}$	spontaneous emission coefficients of vibration level v of CO

a	radius of laser tube
a_0	Bohr radius
B_{s0}	rotational constant for ground state of species s
$B(u)$	quantity defined by equations (B7)
BVT_v^{st}	backward vibration-translation rate coefficient defined by equation (A17)
B_v	rotational constant of vibrational level v of CO defined by equation (C8)
b_{st}	quantity defined in equations (A3)
$C(u)$	quantity defined in equations (B7)
c	velocity of light
$D(u)$	quantity defined in equations (B7)
D_v	quantity defined in equation (C9)
d_s, d_t	collision diameter of Lennard-Jones potential for species s and t
d_{st}	collision diameter defined in equation (A8)
E	electric field strength
$\vec{E}$	electric field strength vector
E_v^s, E_v^t	energy of vibrational level v of species s and t
e	electronic charge of electron
F	adiabaticity factor defined by equations (A4) and (A5)
F_v	quantity defined by equation (C7)
f_c	collision frequency defined in equations (C4)

$f(u)$	electron energy distribution function
G_s	anharmonic vibrational energy function defined by equations (16)
$g(u)$	function defined by equation (B11)
H	specific enthalpy of gas mixture defined by equation (15)
H_o	specific enthalpy of gas mixture at tube entrance
h	Planck's constant
h_s	specific enthalpy of species s
$h_{s,v}$	specific enthalpy of vibrational level v of species s
I	arc current
I_s, I_t	ionizational potential of species s and t
$I_{v,J}$	intensity
J	rotation quantum number
j	current density
$\vec{j}$	current density vector
K_D	quantity defined in equations (B8)
K_Q	quantity defined in equations (B8)
K_{sD}	quantity defined in equations (B3)
K_{sQ}	quantity defined in equations (B5)
K_{VT}^{st}	empirical constant in equation (A2)
K_{VV}^{st}	empirical constant in equation (A21)

k	Boltzmann's constant
L	length of laser tube
L_{opt}	length of optical axis
$L^{st}_{v,v'}$	long-range vibration-vibration rate coefficient defined by equation (A20)
ℓ_{st}	empirical constant in equations (A3)
M	average mass defined in equations (B8)
m_e	electron mass
m_s	mass of species s
m_t	quantity defined by equations (A3)
$\dot{m}$	total mass flow rate
$\dot{m}_s$	mass flow rate of species s
N	total number density
N_e	density of electron
N_s	number density of species s
$N_{s,J}$	number density of species s with rotational quantum number J
$N_{s,v}$	number density of species s in vibrational level v
$P(J)$	rotational branch of a given vibrational transition
P_v	power from vibrational level v
$P^s_{v,J}$	rate for electron impact excitation from vibrational level J

$P^s_{v,v'}$	electron impact vibrational excitation rate for species s defined by equations (B20) and (B21)
p	static pressure
$p\tau_{st}$	relaxation time of species s by species t
Q_ℓ	energy loss due to lasing
Q_s	energy loss by spontaneous emission
Q_{sJ}	electron inelastic cross section with energy loss u_{sJ} for species s
Q^*_{sJ}	electron inelastic cross section with energy gain u_{sJ} for species s
Q_{sm}	momentum transfer cross section for electrons in species s
Q_{sv}	electron inelastic cross section with energy loss u_{sv} for species s
Q_T	total heat loss
Q_w	heat loss by wall transfer
Q_1, Q_2	cross sections defined in equations (B8)
$\vec{q}$	heat flux vector
R_s, R_t	particle rate of production of species s and t
$R_{s,v}$	particle rate of production of vibrational level v of species s
$\left\lvert \frac{R^s_{v,v-1}}{R^s_{1,0}} \right\rvert^2$	vibrational matrix element of species s
R_∞	ionizational energy of ground state of Bohr atom
r	distance in radial direction
r_1, r_2	mirror reflectivities
S_v	line shape factor defined by equation (C3)

$S^{st}_{v,v'}$	short-range vibration-vibration rate coefficient defined by equation (A21)
s,t	species
T	temperature
T^{st}_{crit}	critical temperature used in equation (A10)
T_e	electron temperature
T^*_{st}	characteristic temperature defined in equations (A3)
$T_{s,v}$	vibrational temperature of species s defined by equation (8)
T_w	wall temperature of laser tube
U	flow velocity
$\vec{U}$	vector flow velocity
U_m	mean flow velocity
u	electron energy in electron volts
u_{sJ}	electron energy loss or gain in Jth inelastic collision process with species s
u_T	gas temperature in electron volts defined in equations (B8)
V	arc voltage
VT^{st}_v	vibration-translation rate coefficient defined by equations (A2) and (A10)
$VV^{st}_{v,v'}$	vibration-vibration rate coefficient defined by equation (A19)
v	vibration quantum number
v^*_s	vibration distribution truncation level of species s
v_T	number of lasing transitions

W_{st} empirical constant used in equation (A20)

w electron drift velocity defined by equation (B15)

X_s mole fraction of species s

x quantity defined in equations (C4)

Y_s mass fraction of species s, $\frac{\rho N_s}{m_s}$

$Y_{s,v}$ mass fraction of species s in vibration level v

y variable used in equations (A4) and (A5)

y_v^{st} quantity defined in equations (A3)

$y_{v,v'}^{st}$ quantity defined in equation (A22)

Z_{st} collision frequency defined by equation (A7)

α_v threshold gain for transition v

β_s mole fraction defined in equations (B8)

Γ gamma function

$\gamma_{v,J}$ gain coefficient defined by equation (C1)

ΔE energy loss found in equations (A1) and (A18)

$\Delta\nu_c$ Lorentz half-width defined in equations (C4)

$\Delta\nu_D$ Doppler half-width defined in equations (C4)

δ_s quantity defined in equations (A3)

ϵ_s, ϵ_t potential well depth of Lennard-Jones potential of species s or t

ϵ_{st} potential well depth defined in equation (A6)

η	variable used in equation (A23)
θ_{sD}	electric dipole moment of species s
θ_{sQ}	electric quadrupole moment of species s
θ_v^s	characteristic temperature defined in equations (A3)
$\theta_{v,v'}^{st}$	temperature defined in equation (A22)
λ	quantity defined in equations (B8)
λ_m	mean thermal conductivity of mixture defined by equation (18)
λ_s	thermal conductivity of species s
μ	electron mobility defined by equation (B16)
μ_{st}	reduced mass defined in equations (A3)
ν_v	frequency defined by equation (C2)
$\nu_{v,J}$	frequency defined by equation (C6)
ρ	density
σ_{opt}^{st}	optical cross section
σ_{sD}	quantity defined in equations (B3)
σ_{sQ}	quantity defined in equations (B5)
$\Omega^{(2,2)}$	quantity defined by equation (A9)
$\omega_e, \omega_e x_e, \omega_e y_e, \omega_e z_e$	vibrational constants in equations (16)

An arrow over a symbol denotes a vector quantity. An asterisk denotes the largest possible value. A prime denotes a variation of any term. The subscript max denotes a maximum value.

ANALYTICAL FORMULATION

The laser system modeled in this analysis is based on the experimental work of Sidney et al. (ref. 9) and is shown schematically in figure 1. The discharge tube is made of pyrex and is 2.54 cm in diameter and 92 cm long. Annular stainless-steel electrodes, 2.54 cm in diameter and 8 cm long, are fitted to the tube ends and calcium fluoride Brewster angle windows are placed on the electrode ends. The tube, exclusive of the electrodes, is immersed in a liquid nitrogen bath in a bakelite container. Compartments at either end of the container were designed with adjustable liquid nitrogen leaks to control the temperature of the electrodes. The constituent gases are premixed in an upstream reservoir and are introduced at the cathode and exhausted near the anode. The pressure drop in the tube was negligibly small for the operating conditions of the experiment.

In analyzing the experiment, molecules in different vibrational quantum states are treated as separate species. For such a multicomponent mixture, the governing equations are the electron Boltzmann equation, the conservation of species equations, the overall continuity, momentum, and energy equations, and the equation of state.

The electron Boltzmann equation is

$$\frac{E^2}{3}\frac{d}{du}\left[\frac{u}{\sum_s (N_s Q_{sm})}\frac{df}{du}\right] + \sum_s \left[\frac{2m_e}{m_s}\frac{d}{du}\left(u^2 N_s Q_{sm} f\right)\right]$$

$$+ \sum_s \left[\frac{2m_e}{m_s}\frac{kT}{e}\frac{d}{du}\left(u^2 N_s Q_{sm}\frac{df}{du}\right)\right] + \sum_s N_s\left\{\sum_J \left[(u + u_{sJ})\, f(u + u_{sJ})\, Q_{sJ}(u + u_{sJ})\right]\right.$$

$$- u\, f(u) \sum_J \left[Q_{sJ}(u)\right] + \sum_J \left[(u - u_{sJ})\, f(u - u_{sJ})\, Q^*_{sJ}(u - u_{sJ})\right]$$

$$\left. - u\, f(u) \sum_J \left[Q^*_{sJ}(u)\right]\right\} = 0 \qquad (1)$$

This equation is considered in detail in appendix B. The electron temperature and the electron number density are determined from the current density and the electron distribution function as

$$T_e = \frac{2}{3}\frac{e}{k}\int_0^\infty u^{3/2} f(u)\, du \tag{2}$$

and

$$N_e = \frac{j}{ew}$$

$$w = \mu E = \mu N \frac{E}{N}$$

$$E = \frac{V}{L}$$

where

$$\mu = -\frac{1}{3N}\left(\frac{2e}{m_e}\right)^{1/2} \int_0^\infty \frac{u}{\sum X_s Q_{sm}} \frac{df}{du}\, du \tag{3}$$

By use of the steady-state approximation, the conservation of species equation for a given species s reduces to

$$R_s = 0 \tag{4}$$

The species considered are the vibrational levels of CO from $v = 0$ to $v = v^*_{CO}$ and the vibrational levels of N_2 from $v = 0$ to $v = v^*_{N_2}$, where v^*_{CO} and $v^*_{N_2}$ were chosen to be 50.

The kinetic processes assumed to be of importance in developing expressions for the production rates R_s are

(1) Electron impact excitation of vibrational levels 1 to 8 of both CO and N_2

(2) Single quantum vibration-vibration (V-V) exchange collisions
(CO-CO, CO-N_2, N_2-N_2)

(3) Single quantum vibration-translation (V-T) exchange collisions
(CO-CO, CO-He, CO-N_2, N_2-CO, N_2-N_2, N_2-He)

(4) Spontaneous emission of CO ($\Delta v = 1$ and $\Delta v = 2$)

(5) Stimulated emission and absorption of CO.

The cross sections for electron excitation of vibrational levels 9 and 10 for both CO and N_2 were measured by Boness and Schulz. (See ref. 10.) However, because of their small magnitudes, they were not included in this analysis.

For the vth vibrational level of CO,

$$
\begin{aligned}
R_{CO,v} = N_e\left[\sum_{J=0}^{8}\left(N_{CO,J}P_{v,J}^{CO}\right) - N_{CO,v}\sum_{J=0}^{8}\left(P_{v,J}^{CO}\right)\right] + N_{CO,v+1}\left[\sum_{J=0}^{v_{CO}^{*}}\left(N_{CO,J}VV_{v+1,J}^{CO\text{-}CO}\right)\right. \\
\left. + \sum_{J=0}^{v_{N_2}^{*}}\left(N_{N_2,J}VV_{v+1,J}^{CO\text{-}N_2}\right) + \sum_{s}\left(N_s VT_{v+1}^{CO\text{-}s}\right) + A_{v+1}^{(1)}\right] \\
- N_{CO,v}\left[\sum_{J=0}^{v_{CO}^{*}}\left(N_{CO,J+1}VV_{J+1,v}^{CO\text{-}CO} + N_{CO,J}VV_{v,J}^{CO\text{-}CO}\right)\right. \\
+ \sum_{J=0}^{v_{N_2}^{*}}\left(N_{N_2,J+1}VV_{J+1,v}^{N_2\text{-}CO} + N_{N_2,J}VV_{v,J}^{CO\text{-}N_2}\right) + \sum_{s}N_s\left(BVT_{v+1}^{CO\text{-}s} + VT_{v}^{CO\text{-}s}\right) \\
\left. + A_v^{(1)} + A_v^{(2)}\right] + N_{CO,v-1}\left[\sum_{J=0}^{v_{CO}^{*}}\left(N_{CO,J+1}VV_{J+1,v-1}^{CO\text{-}CO}\right)\right. \\
\left. + \sum_{J=0}^{v_{N_2}^{*}}\left(N_{N_2,J+1}VV_{J+1,v-1}^{N_2\text{-}CO}\right) + \sum_{s}\left(N_s BVT_{v}^{CO\text{-}s}\right)\right] \\
+ N_{CO,v+2}\,A_{v+2}^{(2)} + \frac{\gamma_{v+1,J}I_{v+1,J}}{h\nu_{v+1,J}} - \frac{\gamma_{v,J}I_{v,J}}{h\nu_{v,J}}
\end{aligned}
\tag{5}
$$

and for the vth vibrational level of N_2

$$R_{N_2,v} = N_e\left[\sum_{J=0}^{8}\left(N_{N_2,J}P_{Jv}^{N_2}\right) - N_{N_2,v}\sum_{J=0}^{8}\left(P_{vJ}^{N_2}\right)\right] + N_{N_2,v+1}\left[\sum_{J=0}^{v_{N_2}^*}\left(N_{N_2,J}VV_{v+1,J}^{N_2-N_2}\right)\right.$$

$$\left. + \sum_{J=0}^{v_{CO}^*}\left(N_{CO,J}VV_{v+1,J}^{N_2-CO}\right) + \sum_{s}\left(N_s VT_{v+1}^{N_2-s}\right)\right] - N_{N_2,v}\left[\sum_{J=0}^{v_{N_2}^*}\left(N_{N_2,J+1}VV_{J+1,v}^{N_2-N_2}\right.\right.$$

$$\left. + N_{N_2,J}VV_{v,J}^{N_2-N_2}\right) + \sum_{J=0}^{v_{CO}^*}\left(N_{CO,J+1}VV_{J+1,v}^{CO-N_2} + N_{CO,J}VV_{v,J}^{N_2-CO}\right)$$

$$\left. + \sum_{s} N_s\left(BVT_{v+1}^{N_2-s} + VT_v^{N_2-s}\right)\right] + N_{N_2,v-1}\left[\sum_{J=0}^{v_{N_2}^*}\left(N_{N_2,J+1}VV_{J+1,v-1}^{N_2-N_2}\right)\right.$$

$$\left. + \sum_{J=0}^{v_{CO}^*}\left(N_{CO,J+1}VV_{J+1,v-1}^{CO-N_2}\right) + \sum_{s}\left(N_s BVT_v^{N_2-s}\right)\right] \tag{6}$$

These expressions contain terms which involve N_{CO,v_{CO}^*+1} and $N_{N_2,v_{N_2+1}^*}$. If these terms are simply set to zero, then false inversions can occur on the upper levels. To eliminate this problem, the number densities for the $v_{CO}^* + 1$ and the $v_{N_2}^* + 1$ levels are estimated by assuming that the population distribution in the last few levels can be approximated by a Boltzmann distribution; that is,

$$N_{s,v_s^*+1} = N_{s,v_s^*}\exp\left(-\frac{E_{v_s^*+1}^{s} - E_{v_s^*}^{s}}{kT_{s,v}}\right) \tag{7}$$

where

$$T_{s,v} = \frac{-\left(E_{v_s^*}^{s} - E_{v_s^*-1}^{s}\right)}{k\log_e\left(\frac{N_{s,v_s^*}}{N_{s,v_s^*-1}}\right)} \tag{8}$$

This method was first used by Lordi et al. (See ref. 11.)

The various V-T and V-V rate coefficients used in equations (5) and (6) are discussed in appendix A. The electron vibrational excitation rates P^S_{iJ} are defined in appendix B. The only excitation cross sections which have been measured experimentally for CO and N_2 are those for excitation from the ground state (ref. 10). Chen (ref. 12) has calculated theoretical cross sections for vibrational excitation from levels $v = 1, 2, 3,$ and 4 for N_2. By using his results, Abraham and Fisher (ref. 13) have demonstrated that if electron vibrational excitation processes have the same Δv, then they have approximately the same rate as the excitation process from $v = 0$. Thus, it is assumed that

$$P^S_{v,v+1} = P^S_{0,1} \qquad (v = 1 \text{ to } 7) \tag{9}$$

The spontaneous emission coefficients for CO were generated from the matrix elements of Young and Eachus (ref. 14). However, they calculated the matrix elements only up to $v = 24$. The elements for the higher levels were generated by extending the calculations of reference 14 to $v = 50$. The dipole moment vibrational elements and the spontaneous emission coefficients are given in table I.

The overall continuity equation is written as

$$\rho UA = \dot{m} \tag{10}$$

whereas the overall momentum equation reduces to

$$\nabla P = 0 \tag{11}$$

The overall energy equation has the form

$$\nabla \cdot \left[\rho \vec{U}\left(H + \frac{U^2}{2}\right) + \vec{q}\right] = \vec{j} \cdot \vec{E} \tag{12}$$

For the steady-state approximation employed here, this equation can be integrated to give

$$\dot{m}(H - H_0) = IV - Q_T \tag{13}$$

The total heat loss Q_T is expressed as the sum of losses due to conduction to the wall, spontaneous emission, and lasing. Thus, equation (13) becomes

$$\dot{m}(H - H_0) = IV - Q_W - Q_S - Q_\ell \tag{14}$$

TABLE I. - DIPOLE MATRIX ELEMENTS AND SPONTANEOUS EMISSION COEFFICIENTS OF CO

v	$\left\|R^{CO}_{v,v-1}/R^{CO}_{1,0}\right\|^2$	$A^{(1)}_v$, sec^{-1}	$A^{(2)}_v$, sec^{-1}	v	$\left\|R^{CO}_{v,v-1}/R^{CO}_{1,0}\right\|^2$	$A^{(1)}_v$, sec^{-1}	$A^{(2)}_v$, sec^{-1}
1	1.000	33.4	-----	26	19.698	227.6	201.8
2	1.995	64.2	0.9	27	19.987	220.0	212.2
3	2.985	92.5	2.7	28	20.241	211.9	222.2
4	3.968	118.4	5.3	29	20.460	203.7	231.9
5	4.945	141.9	8.8	30	20.644	195.4	241.1
6	5.913	163.3	13.0	31	20.793	186.9	249.9
7	6.867	182.3	18.0	32	20.908	178.4	258.2
8	7.816	199.4	23.7	33	20.988	169.8	265.9
9	8.739	214.2	30.2	34	21.033	161.3	273.0
10	9.660	227.4	37.2	35	21.044	152.9	279.6
11	10.560	238.7	45.0	36	21.020	144.5	285.5
12	11.436	248.0	53.4	37	20.961	136.3	290.7
13	12.285	255.5	62.3	38	20.867	128.2	295.3
14	13.104	261.3	71.6	39	20.738	120.4	299.2
15	13.898	265.5	81.4	40	20.575	112.7	302.4
16	14.656	268.2	91.6	41	20.377	105.2	304.9
17	15.368	269.2	102.3	42	20.144	98.0	306.8
18	16.038	268.8	113.0	43	19.877	91.0	307.9
19	16.644	266.8	124.1	44	19.575	84.2	308.3
20	17.220	263.8	135.3	45	19.238	77.8	308.0
21	17.735	259.6	146.6	46	18.866	71.6	307.1
22	18.227	254.8	157.8	47	18.459	65.6	305.5
23	18.676	249.1	169.1	48	18.017	60.0	303.2
24	19.056	242.4	180.2	49	17.540	54.7	300.4
25	19.375	235.0	190.8	50	17.028	49.6	296.9

The specific enthalpy of the mixture is given by

$$H = Y_e h_e + Y_{He} h_{He} + \sum_{v=0}^{v_{CO}^*} Y_{CO,v} h_{CO,v} + \sum_{v=0}^{v_{N_2}^*} Y_{N_2,v} h_{N_2,v} \tag{15}$$

where

$$\left.\begin{aligned}
h_e &= \frac{5}{2}\frac{kT_e}{m_e} + \frac{I_{CO}}{m_e} \\
h_{He} &= \frac{5}{2}\frac{kT}{m_{He}} \\
h_{CO,v} &= \frac{7}{2}\frac{kT}{m_{CO}} + \frac{E_v^{CO}}{m_{CO}} \\
h_{N_2,v} &= \frac{7}{2}\frac{kT}{m_{N_2}} + \frac{E_v^{N_2}}{m_{N_2}} \\
E_v^S &= hc\left[G_s(v) - G_s(0)\right] \\
G_s(v) &= \omega_e\left(v + \frac{1}{2}\right) - \omega_e x_e\left(v + \frac{1}{2}\right)^2 + \omega_e y_e\left(v + \frac{1}{2}\right)^3 + \omega_e z_e\left(v + \frac{1}{2}\right)^4
\end{aligned}\right\} \tag{16}$$

The units of $G_s(v)$ are cm^{-1} and the vibrational constants for CO and N_2 found in equations (16) are given in table II.

TABLE II.- VIBRATIONAL CONSTANTS OF CO AND N_2

[From refs. 15 and 16]

	CO	N_2
ω_e	2169.82	2359.61
$\omega_e x_e$	13.292	14.456
$\omega_e y_e$	.01082	.00751
$\omega_e z_e$	.000052	-.000509

Heat loss to the wall can be expressed as (ref. 17)

$$Q_w = 6\pi\left(T - T_w\right)\lambda_m L \tag{17}$$

where

$$\lambda_m = 0.5\left[\sum X_s\lambda_s + \left(\sum \frac{X_s}{\lambda_s}\right)^{-1}\right] \tag{18}$$

Equation (17) is developed in reference 17 on the assumption that the average or bulk temperature of a fully developed flow in a tube of radius a is defined as

$$T = \frac{1}{a}\int_0^a T(r)\,dr \tag{19}$$

But the usual definition of the average gas temperature (ref. 18) is

$$T = \frac{\int T(r)\,U(r)\,dA}{\int U(r)\,dA} \tag{20}$$

Thus, the assumption of a constant $U(r)$, which is implied in reference 17, would seem to indicate that this expression for Q_w is incorrect. However, for fully developed pipe flow (ref. 18),

$$U(r) = U_m\left[1 - \left(\frac{r}{a}\right)^2\right] \tag{21}$$

Using equation (21) in equation (20) leads to the expression for Q_w in equation (17). The thermal conductivities used in equation (17) were obtained from reference 19.

Spontaneous emission losses are given by

$$Q_s = AL\left[\sum_{v=1}^{v_{CO}^*} N_{CO,v}A_v^{(1)}\left(E_v^{CO} - E_{v-1}^{CO}\right) + \sum_{v=2}^{v_{CO}^*} N_{CO,v}A_v^{(2)}\left(E_v^{CO} - E_{v-2}^{CO}\right)\right] \tag{22}$$

and the laser power output is

$$Q_\ell = AL\sum \gamma_{v,J}\,I_{v,J} \tag{23}$$

Finally, the equation of state for the system can be written as

$$p = kN_eT_e + kNT \tag{24}$$

When operating in the lasing mode, the intensities of each transition $I_{v,J}$ assume values such that the gain coefficient $\gamma_{v,J}$ for each transition satisfies the threshold condition (ref. 20)

$$\gamma_{v,J} = \frac{-\log_e (r_1 r_2)}{2L_{opt}} \tag{25}$$

This condition is a statement of the fact that the intensity gain on a line just equals the intensity loss on that line for a round trip through the discharge region. If the losses are of a magnitude such that the gain coefficient for a given transition is less than the threshold value, no lasing can occur on that line.

An expression for the gain coefficient including the effects of both Doppler and pressure broadening is given in appendix C. The development of this expression includes the assumption of the equilibrium of the rotational states at the gas temperature. Thus, it is not possible to predict transitions on more than one rotational line in a given vibrational band. Therefore, it is assumed that for a given vibrational band, lasing occurs only on the P(J) branch corresponding to the maximum small signal gain coefficient.

Equations (1), (4), (10), (11), (14), and (24) together with the expressions for the electron temperature and the electron number density given by equations (2) and (3) form the basic system to be solved. When the system operates in an oscillator mode, this system of equations is supplemented by threshold conditions given by equation (25) equal in number to the lasing transitions.

METHOD OF SOLUTION

The governing system of equations consists of the electron Boltzmann equation, which is a difference differential equation, and $3 + v^*_{CO} + v^*_{N_2} + v_T$ nonlinear algebraic equations corresponding to the number densities of the v^*_{CO} vibrational levels of CO plus the ground state, the number densities of the $v^*_{N_2}$ vibrational levels of N_2 plus the ground state, the gas temperature, and the v_T lasing intensities. For small signal gain calculations, the intensities are set equal to zero and thus the last v_T equations are not needed. The electron Boltzmann equation is integrated numerically by using a constant-step-size, fourth-order, Adams-Moulton predictor-corrector method. The system of nonlinear algebraic equations is solved numerically by using a Newton-Raphson technique.

The procedure used in obtaining a complete solution for a given set of operating conditions is summarized as follows:

(1) For the given composition, the electron Boltzmann equation is solved for a range of E/N values to obtain the electron distribution function. This solution is then

used to calculate the electron vibrational excitation rates which are needed in the rate equations. The electron temperature and mobility are also calculated. This information is stored for later use.

(2) Next, a calculation of the small signal gain coefficients is carried out. With the given operating conditions, that is, composition, pressure, flow rates, arc voltage and current, and tube dimensions, an initial value for the temperature and an initial vibrational distribution for the CO and N_2 molecules are assumed. The corresponding electron temperature is determined by interpolation from the table generated in step (1). A similar procedure is employed to determine the vibrational excitation rates and mobility. The electron number density can then be found from equation (3). The V-V and V-T rates for the various collisions are computed at the assumed temperature. By using this information, the initial values of the rate equations and the energy equation together with all their partial derivatives which are needed for the Newton-Raphson iteration scheme are calculated. After each iteration, the procedure of determining an electron temperature and all parameters associated with it and a set of V-V and V-T rates for the new temperature is repeated. The iteration is continued until convergence on all variables to a relative error of 10^{-3} is achieved.

For the small signal gain calculations, all intensities are set to zero and thus the equations for the threshold condition are omitted. The converged values of number densities and temperature are used to calculate small signal gain coefficients for the vibrational-rotational transitions of interest. For each vibrational band, the gains are calculated for a number of $P(J)$ transitions and the value of the maximum gain on each band together with the J number of the rotational transition on which it occurs are retained for use in step (3).

(3) Finally, an intensity calculation is carried out. In this case, it is necessary to introduce the threshold condition given by equation (25) for each intensity to be calculated. Thus, v_T additional unknowns and v_T additional equations are added to the system.

The lines for which small signal gain coefficients are maximum for a given band may oscillate if their gain coefficients are greater than or equal to the threshold value. Such lines are determined by comparing the maximum gain values for each band calculated in step (2) to the threshold gain value.

The resulting system of equations is solved again by a Newton-Raphson technique. If a negative intensity appears in the converged solution, it is dropped, together with its associated threshold condition, and the solution procedure is repeated. When a converged set of all positive intensities is obtained, the power from each line is calculated from the expression

$$P_V = AL\alpha_V I_{V,J} \tag{26}$$

The power from all lines is summed to obtain the total laser power.

An important point to remember when calculating intensities is that the J number which specifies the P(J) transition with the maximum small signal gain coefficient on a given vibrational band is not necessarily the same as for the case when lasing is not present. Thus, after each iteration, a small signal gain calculation is performed and the J numbers associated with each lasing transition are adjusted accordingly. A typical example of this shift can be seen in table III corresponding to the conditions for case 1. (See table IV in "Results and Discussion.")

TABLE III.- COMPARISON OF J VALUES FOR SMALL SIGNAL GAIN CALCULATIONS AND INTENSITY CALCULATIONS FOR CASE 1

Vibrational band	Gain calculations	Intensity calculations
4 → 3	P(10)	P(10)
5 → 4	P(8)	P(10)
6 → 5	P(7)	P(10)
7 → 6	P(7)	P(9)
8 → 7	P(7)	P(9)
9 → 8	P(7)	P(8)
10 → 9	P(7)	P(8)
11 → 10	P(7)	P(8)
12 → 11	P(7)	P(8)
13 → 12	P(7)	P(8)
14 → 13	P(7)	P(7)

As was indicated earlier, 50 vibrational levels were carried for both CO and N_2 in all calculations. Provision was made for calculating a maximum of 25 lasing intensities. However, typically, it was not necessary to calculate more than 14 corresponding to vibrational transitions from the 3 → 2 up to the 16 → 15.

RESULTS AND DISCUSSION

The primary processes of pumping energy into the CO vibrational levels are through electron excitation of the lower levels and V-V pumping of the higher levels. Radiative decay and V-T collisions are the primary processes for deactivating the vibrational

states, and these processes are dominant for the higher levels. Thus, to promote lower level transitions, one needs to increase the efficiency of the lower level excitations and V-T collisions and reduce the efficiency of V-V pumping. To reduce the efficiency of V-V pumping, one needs to reduce the pressure (or flow rate) and partial pressure of CO in the system. The presence of a large fraction of He increases the efficiency of the V-T collisions and helps maintain a low gas temperature. Nitrogen was found to be beneficial in promoting low level transitions in the experiments of Djeu (refs. 3 and 4); he attributed its role to the fact that $v \rightarrow v - 1$ transitions in CO are in resonance with the $v + 6 \rightarrow v + 5$ transitions in N_2.

All calculations performed in this analysis are based on a wall temperature of 77 K and mirror reflectivities of 1.0 and 0.84. The other parameters employed in the calculations, which correspond to the range of operating conditions employed in the experiment (ref. 9), are listed in table IV.

TABLE IV.- OPERATING CONDITIONS FOR THE CASES CONSIDERED

Case number	$\dot{m}_{CO}$, 10^{-5} g/sec	$\dot{m}_{N_2}$, 10^{-5} g/sec	$\dot{m}_{He}$, 10^{-4} g/sec	Arc current, mA	Arc voltage, kV	Tube pressure, torr
1	1.96	0.00	3.91	7.3	3.4	3.5
2	5.85	.00	11.73	6.6	4.8	6.3
3	9.77	.00	19.55	6.0	6.0	8.2
4	1.92	3.81	3.83	2.0	4.0	3.5
5	5.76	11.42	11.50	6.4	5.2	6.3
6	9.60	19.04	19.16	5.7	6.6	8.2
7	1.68	26.78	3.38	6.3	5.4	3.5
8	5.04	80.36	10.15	5.3	7.4	6.3
9	8.39	133.90	16.92	4.4	9.2	8.2
10	1.68	26.80	3.88	6.6	4.8	3.8
11	5.04	80.40	10.20	5.4	7.2	6.8
12	8.39	134.00	16.90	4.2	9.6	9.0
13	3.32	26.60	3.35	6.5	5.0	3.8
14	9.96	79.60	10.00	5.2	7.6	6.8
15	16.60	133.00	16.80	3.9	10.2	9.0
16	6.54	26.20	3.31	6.4	5.2	3.8
17	19.60	78.80	9.93	5.1	7.8	6.8
18	32.70	131.00	16.50	3.8	10.4	9.0
19	12.60	25.30	3.19	6.4	5.2	3.8
20	37.90	75.80	9.57	5.1	7.8	6.8
21	63.20	126.00	16.00	3.7	10.6	9.0
22	23.80	23.80	3.00	6.1	5.8	3.8
23	71.20	71.20	8.98	4.9	8.2	6.8
24	119.00	119.00	15.00	3.2	11.6	9.0

The effect of N_2 fraction on the maximum small signal gain coefficient is seen in figure 2. The numbers associated with the various points indicate the P-branch transition at which the gain coefficient is maximum. As is seen from figure 2, N_2 has the overall effect of increasing the efficiency of all vibrational excitations. The primary reason for this behavior is attributed to the decrease in the electron temperature from 28 000 K in the absence of N_2 to 13 600 K in the presence of N_2 as is seen in figure 21. This decrease in the electron temperature results in more electrical power being transferred to the lower vibrational levels of both CO and N_2. (See ref. 21.) In addition, as the number of N_2 molecules is increased, the calculations indicate that the percentage of excited N_2 molecules for $v > 3$ increases; this increase helps pump the lower CO levels because $v + 6 \rightarrow v + 5$ transitions in N_2 are in resonance with $v \rightarrow v - 1$ transitions in CO. This mechanism, however, is secondary to the effect of the electron temperature.

As is seen in figure 2, increasing the N_2 fraction favors the appearance of transitions at low-lying bands and low rotational numbers. This condition explains the behavior of the relative intensity indicated in figure 3 which shows low-lying transitions are favored with increasing N_2 concentration.

The effect of CO on low-lying transitions is discussed next. Increased CO fraction is accompanied by an increase in the V-V pumping or energy transfer from lower to upper levels. This increase dominates all other mechanisms responsible for pumping the lower levels and is the reason for the decrease in the maximum gain coefficients of the low-lying bands with increase in CO concentration shown in figure 4 and the disappearance of the low-lying transitions in figure 5.

Figures 6 and 7 show the effect of pressure (or, equivalently, the flow rate) on the maximum small signal gain coefficients and the relative intensities. An increase in the pressure for a given mixture results in an increase in the number of CO molecules in the system and thus improves the efficiency of the CO V-V pumping mechanism. The calculations also indicate that at higher pressures, more electrical power is being transferred to the lower levels of CO while at the same time the percentage of excited N_2 molecules decreases. Thus, N_2-CO V-V pumping is reduced. These considerations are responsible for the decrease in the maximum small signal coefficient and the relative intensities of the low-lying levels as the pressure increases.

In figures 8 and 9 a comparison of theory with experiment is presented. Figure 8 shows a typical plot of the relative intensity as a function of the upper vibrational levels; the numbers associated with the various points indicate the P-branch at which the intensity is maximum. In general, the predictions of the levels at which the peak intensity occurs, the relative magnitudes of the intensities, and the rotational numbers at which the intensity is maximum in a given band are in good agreement with experiment.

However, comparison of measured and calculated gain coefficients for the low-lying line 5→4(9) indicated in figure 9 shows that the theory overpredicts the measurements by a factor of two. The discrepancy between calculated and measured gain coefficients in CO lasers was discussed by Greene and Harris. (See ref. 22.) They showed that their calculations of the small signal gain coefficient for low temperature e-beam sustained continuous wave CO-Ar lasers, using the expression given in reference 7, agree with experiment if they discard hard sphere models for the optical broadening cross sections and employ instead cross sections which have the dependence on the rotational number J and the gas temperature suggested by Varanasi. (See ref. 23.)

In this work the cross sections given in reference 24 are employed. These cross sections allow for the dependence on J but not on temperature. Allowing for the temperature dependence suggested in reference 23 reduces the calculated gain coefficient by 25 percent. Thus, the discrepancy does not result from failing to use the proper gain coefficient or the proper cross section.

The discrepancy can be attributed to a number of factors, the most important of which is that the theory assumed a rather clean experiment in which impurities such as H_2O, CO_2, and the nitrogen oxides were nonexistent. This, of course, is not a realistic assumption. Another reason for the discrepancy is that O_2 was treated as an inert gas in the theory; O_2 was added in the experiment to prevent the dissociation of CO and the formation of carbon. Because the calculations employed the experimentally determined electric field and current, the effect of O_2 on performance cannot be attributed to a change in the electron distribution function resulting from changes in E/N which accompany the addition of O_2. (See ref. 25.) It is believed that the presence of O_2 results in the formation of NO and this can deactivate the excited levels of CO.

In addition to these effects, recent analysis of gain measurements has indicated that measured values of gain coefficient can be substantially below the true value; this condition takes place in the presence of internal gain saturation and during the employment of large collector apertures. (See ref. 26.) The situation was further compounded by the fact that for low CO concentrations, the laser operation was not very stable. This instability could be a result of an ionization instability. (See refs. 27 and 28.)

CONCLUDING REMARKS

The theory presented here suggests that low transitions in CO laser systems can be achieved at low flow rates (or pressures) for rather low CO partial pressures relative to those of He and N_2. The primary role of N_2 appears to be the reduction of the electron temperature to a level where the transfer of electric power to the lower vibrational states

is optimum. The trends predicted by the theory are substantiated by experiment. However, further analysis is needed to assess the role of impurities that inherently exist in any given experiment.

Langley Research Center
National Aeronautics and Space Administration
Hampton, Va. 23665
March 5, 1976

APPENDIX A

VIBRATIONAL RATE COEFFICIENTS

The rate coefficients for vibration-translation (V-T) and vibration-vibration (V-V) exchange collisions used in this analysis are calculated as the product of a transition probability (TP) and an elastic collision frequency. The expressions contain variable parameters which may be adjusted to obtain the best possible agreement with experimental rate measurements.

The V-T rate expression used is based on the Schwartz-Slawsky-Herzfeld (SSH) theory (ref. 29, pp. 260-350) with suitable modifications. A typical V-T exchange collision can be described by

$$AB(v = n) + C \rightleftharpoons AB(v = n - 1) + C + \Delta E(n) \tag{A1}$$

where A, B, and C represent different molecules and $\Delta E(n)$ is the energy lost in the collision which is converted into heat. In SSH theory, the vibrating molecules are treated as harmonic oscillators. Keck and Carrier (ref. 30) substituted a Morse oscillator model and also introduced an empirical fit for the adiabaticity factor (which shall be defined later). This latter modification allows the modeling of collision types ranging from impulsive to adiabatic energy exchange. Bray (ref. 31) was the first to incorporate these modifications of SSH theory into an analytical study of vibrational relaxation processes. Since that time, many theoretical CO laser studies (refs. 4 to 6 and 13) have made use of his work.

A further modification to SSH theory was made necessary by a consideration of intermolecular interaction potentials between colliding molecules. Simple SSH theory assumes only an exponential repulsive potential between the molecules, but, in reality, an attractive force is also present. This attractive well can have a significant effect especially at low temperatures. (See refs. 32 and 33.) Shin (ref. 32) has shown that the TP for a Morse potential, which has an attractive well and also provides a fairly good approximation to the true intermolecular potential, can be obtained from the TP of the exponential repulsive potential of SSH theory by means of a multiplicative correction factor.

After applying these corrections to the expressions for the V-T rates from SSH theory, the following results are obtained:

APPENDIX A

$$VT_v^{st} = K_{VT}^{st} TZ_{st} \frac{v}{(1 - v\delta_s)} \exp\left(\frac{\theta_v^s}{2T}\right) F\left(y_v^{st}\right) \exp\left[\frac{4}{\pi\sqrt{T_{st}^*}}\left(y_v^{st}\right)^{1/3} + \frac{16}{3\pi^2 T_{st}^*}\right] \tag{A2}$$

where

$$\left.\begin{aligned} \theta_v^s &= \frac{E_v^s - E_{v-1}^s}{k} \\ y_v^{st} &= \left[\frac{b_{st}\left(\theta_v^s\right)^2}{8T}\right]^{1/2} \\ b_{st} &= \frac{16\pi^4 k}{h^2} \mu_{st} \ell_{st} \\ \delta_s &= \left(\frac{\omega_e x_e}{\omega_e}\right)_s \\ \mu_{st} &= \frac{m_s m_t}{m_s + m_t} \\ T_{st}^* &= \frac{T}{\epsilon_{st}} \end{aligned}\right\} \tag{A3}$$

The adiabaticity factor $F\left(y_v^{st}\right)$ can be expressed as

$$F(y) = \frac{1}{2} \exp\left(-\frac{2y}{3}\right)\left[3 - \exp\left(-\frac{2y}{3}\right)\right] \tag{A4}$$

for $0 \leqq y \leqq 21.622$ and as

$$F(y) = 8\sqrt{\frac{\pi}{3}}\, y^{7/3} \exp\left(-3y^{2/3}\right) \tag{A5}$$

for $y > 21.622$. Equation (A4) is Keck and Carrier's (ref. 30) empirical fit and equation (A5) comes from original SSH theory. The exponential term involving T_{st}^* is Shin's (ref. 32) correction factor. The well depth ϵ_{st} can be expressed as

$$\epsilon_{st} = \frac{2\sqrt{\epsilon_s \epsilon_t}\,\sqrt{I_s I_t}}{I_s + I_t} \tag{A6}$$

APPENDIX A

The collision frequency Z_{st} is calculated from the Lennard-Jones potential parameters of the colliding molecules (ref. 34)

$$Z_{st} = d_{st}^2 \Omega^{(2,2)}\left(T_{st}^*\right)\sqrt{\frac{8\pi kT}{\mu_{st}}} \tag{A7}$$

where

$$d_{st} = \sqrt{d_s d_t} \tag{A8}$$

The combining rates found in equation (A6) are from Good and Hope (refs. 35 and 36). The term $\Omega^{(2,2)}(T)$ is given by an empirical curve fit (ref. 37)

$$\Omega^{(2,2)}(T) = \frac{1.16145}{T^{0.14874}} + 0.52487 \exp(-0.7732T) + 2.16178 \exp(-2.43787T) - 6.435 \times 10^{-4}\, T^{0.14874} \sin\left(\frac{18.0323}{T^{0.7683}} - 7.27371\right) \tag{A9}$$

The parameters appearing in equations (A6) and (A8) are given in table V.

TABLE V.- LENNARD-JONES POTENTIAL PARAMETERS

[From refs. 34 and 38]

	d_s, cm	ϵ_s, K	I_s, eV
CO	3.590×10^{-8}	110.0	14.013
N_2	3.617	97.0	15.576
He	2.576	10.22	24.586

In SSH theory, the energy-dependent TP's are obtained from a quantum mechanical distorted wave approximation (refs. 29 and 33). The temperature-dependent TP's are obtained by averaging the energy-dependent TP's over a thermal Boltzmann distribution. At the cryogenic temperatures at which most lasers operate, the energy-dependent TP's are valid. However, the thermal averaging for the temperature-dependent TP's assumes that the energy lost by the oscillating molecules is much less than the kinetic energy of the colliding molecules. At low temperatures, this assumption is not valid and the thermal averaging should be done over the Boltzmann distribution with numerical integration techniques. (See refs. 33 and 39.) However, this procedure is too costly to be used in CO laser studies.

APPENDIX A

Experimental measurements of the V-T rate coefficient for CO deactivation by He and H_2 indicate that when these coefficients are expressed in the proper units $(sec^{-1}\text{-}torr^{-1})$, they are constant below a certain temperature (ref. 40). However, if equation (A2) is used to plot theoretical V-T rate coefficients against temperature (after converting to the proper units[1]), the resulting curve decreases smoothly with decreasing temperature until a certain critical temperature T^{st}_{crit} is reached and then begins to increase with decreasing temperature. Therefore, equation (A2) is used to compute the rate coefficients above the critical temperature. Below that temperature, the rates are calculated from

$$VT_v^{st}(T) = \frac{T}{T^{st}_{crit}} VT_v^{st}\left(T^{st}_{crit}\right) \tag{A10}$$

It has been found that for a given set of constants K^{st}_{VT} and $\ell_{st,}$ the critical temperature decreases slightly as the vibrational level quantum number increases. In this analysis, only the T^{st}_{crit} value for $v = 1$ is used; this procedure has the effect of slightly overestimating the V-T rates for the higher levels at temperatures below T^{st}_{crit}.

The constants K^{st}_{VT} and ℓ_{st} and the T^{st}_{crit} values are presented in table VI. They were obtained by fitting equations (A2) and (A10) to the available experimental rate data. (See refs. 40 to 47.)

TABLE VI.- EMPIRICAL CONSTANTS FOR V-T RATE COEFFICIENTS

	K^{st}_{VT}	ℓ_{st}, Å	T^{st}_{crit}, K
CO-CO	4.4516×10^{-5}	0.203341	135
CO-He	7.1544	.29728	152
N_2-N_2	2.8557	.20328	134
N_2-He	15.476	.3165	145

Figures 10 to 13 show the theoretical rates for CO deactivated by CO and He and for N_2 deactivated by N_2 and He together with the data points used in the curve-fitting

[1]Equation (A2) has units of cm^3/sec and can be converted to $sec^{-1}\text{-}torr^{-1}$ by

$$VT_v^{st}\left(sec^{-1}\text{-}torr^{-1}\right) = \frac{VT_v^{st}\left(cm^3/sec\right)}{1.0355 \times 10^{-19}\ T}$$

process. The solid circle points in figures 10 to 12 do not represent actual data points but were generated from the following empirical curve fits:

$$p\tau_{CO\text{-}CO}(\text{atm-sec}) = 10^{\left(69.3T^{-1/3}-9.64\right)} \tag{A11}$$

for $1372\ K \leqq T \leqq 2915\ K$ (ref. 41),

$$p\tau_{CO\text{-}He}(\text{atm-sec}) = \exp\left(87T^{-1/3} - 19.1\right) \tag{A12}$$

for $580\ K \leqq T \leqq 1500\ K$ (ref. 42), and

$$p\tau_{N_2\text{-}N_2}(\text{atm-sec}) = 10^{\left(102T^{-1/3}-11.24\right)} \tag{A13}$$

for $1900\ K \leqq T \leqq 5600\ K$ (ref. 43). These rate expressions are in the form of a relaxation time $p\tau_{st}$ which is the standard form for giving experimentally measured results. This relaxation time can be expressed in terms of the deactivation rate of the first level of a diatomic molecule (in cm^3/sec) as

$$VT_1^{st} = \frac{1.36236 \times 10^{-22}\ T}{p\tau_{st}\left[1 - \exp\left(-\frac{\theta_1^s}{T}\right)\right]} \tag{A14}$$

The curve fits given by equations (A11), (A12), and (A13) are given in references 41 to 43 instead of tabulated experimental results.

No experimental measurements of the rates of CO deactivated by N_2 and N_2 deactivated by CO are available. Since CO and N_2 have the same molecular weight, SSH theory (ref. 29, pp. 260-350) predicts that the parametric constants appearing in the rate expressions for these reactions will be the same as those for CO deactivated by CO and N_2 deactivated by N_2. Thus, it is assumed that

$$VT_v^{CO\text{-}N_2} = VT_v^{CO\text{-}CO} \tag{A15}$$

and

$$VT_v^{N_2\text{-}CO} = VT_v^{N_2\text{-}N_2} \tag{A16}$$

All backward V-T rate coefficients were obtained from the principle of detailed balancing which gives

$$BVT_v^{st} = VT_v^{st} \exp\left(-\frac{\theta_v^s}{T}\right) \tag{A17}$$

The rate coefficients for vibration-vibration exchange collisions are based on the work of Jeffers and Kelley (ref. 48). They proposed that V-V TP's could be expressed as the sum of two contributions, one a long-range multipole interaction and the other a short-range repulsive force.

Single quantum V-V exchange collisions can be described by

$$AB(v = n) + CD(v = m) \rightleftharpoons AB(v = n - 1) + CD(v = m + 1) + \Delta E(n,m) \tag{A18}$$

Energy from the vibrational mode of one diatomic molecule is transferred to the vibrational mode of another diatomic molecule. If the energy spacings of the vibrational transitions of the two molecules are equal, the energy transfer process is exactly resonant and $\Delta E(n,m)$ is zero, that is, no energy is lost as heat. The quantity $\Delta E(n,m)$ is known as the resonance defect. It is the energy transferred to the translational mode of the gas when the energy spacings of the transitions in the two molecules are not equal. The V-V TP for exactly resonant collisions is high but decreases as the resonance defect increases. V-V transitions with small resonance defects are dominated by the long-range multipole interactions of the colliding molecules (dipole-dipole, dipole-quadrupole, etc.). (See refs. 48 and 49.) The short-range repulsive portion of the intermolecular potential dominates transitions far from resonance. Thus, Jeffers and Kelley (ref. 48) suggested that the V-V TP's could be expressed as the sum of these two contributions, an idea that was independently developed by Caledonia and Center (ref. 50). They utilized the Sharma-Brau theory (ref. 49) to calculate the long-range dipole-dipole contribution to the CO-CO V-V TP's and determined the short-range repulsive force contribution by numerically averaging the energy-dependent Rapp-Englander-Golden transition probabilities (ref. 51) over a thermal Boltzmann distribution. When this theory was applied to CO-CO V-V transitions, good agreement with experimental data (ref. 52) was obtained for temperatures around 300 K. The validity of the basic premise of this model has been questioned (refs. 53 and 54), but a simplified version of it is widely used because it agrees very well with available experimental data.

The V-V rate model used in this analysis is a simplified version of that developed by Jeffers and Kelley. It was first used by Rockwood et al. (ref. 55) who showed that the extremely complicated rate expressions of Sharma and Brau can be approximated very well by a simple Gaussian function of the resonance defect. This function is characterized by two parameters – its magnitude at exact resonance and its half-width. Rockwood et al. (ref. 55) originally assumed constant values for these two parameters, and hence

their expression was valid only at a single temperature. However, the proper temperature dependence (ref. 49) of both the magnitude and half-width of the Gaussian function (ref. 56) is easily introduced. Rockwood et al. (ref. 55) also calculated the short-range repulsive force contribution using a simple expression from modified SSH theory for V-V transitions (refs. 30 and 31).

The V-V rate coefficient expressions, as used in this analysis, are

$$VV^{st}_{v,v'} = L^{st}_{v,v'} + S^{st}_{v,v'} \tag{A19}$$

where

$$L^{st}_{v,v'} = A_{st} \frac{Z_{st}}{T} \left| \frac{R^s_{v,v-1}}{R^s_{1,0}} \right|^2 \left| \frac{R^t_{v'+1,v'}}{R^t_{1,0}} \right|^2 \exp\left(\frac{\theta^{st}_{v,v'}}{2T}\right) \exp\left[-\frac{\left(\theta^{st}_{v,v'}\right)^2}{W_{st}T}\right] \tag{A20}$$

$$S^{st}_{v,v'} = K^{st}_{VV} T Z_{st} \frac{v}{1 - v\delta_s} \frac{v' + 1}{1 - (v' + 1)\delta_t} \exp\left(\frac{\theta^{st}_{v,v'}}{2T}\right) F\left(y^{st}_{v,v'}\right)$$

$$\exp\left[\frac{4}{\pi\sqrt{T^*_{st}}}\left(y^{st}_{v,v'}\right)^{1/3} + \frac{16}{3\pi^2 T^*_{st}}\right] \tag{A21}$$

and

$$\left.\begin{aligned} \theta^{st}_{v,v'} &= \frac{E^s_v - E^s_{v-1} - E^t_{v'+1} + E^t_{v'}}{k} \\ y^{st}_{v,v'} &= \left[\frac{b_{st}\left(\theta^{st}_{v,v'}\right)^2}{8T}\right]^{1/2} \end{aligned}\right\} \tag{A22}$$

and b_{st}, δ_s, δ_t, T^*_{st}, and $F(y)$ may be obtained from equations (A3) to (A5). The vibrational matrix element of the dominant electric multipole moment of molecule s is $\left|R^s_{v,v-1}/R^s_{1,0}\right|^2$. The dipole moment is dominant for CO and the appropriate dipole matrix elements may be found in table I. The electric quadrupole moment is dominant for N_2 and its appropriate matrix elements can be calculated from

$$\left|\frac{R^{N_2}_{v,v-1}}{R^{N_2}_{1,0}}\right|^2 = v\left[(\eta - 2)(\eta - 2v)\right]^2\left[\frac{(\eta - 2v - 1)(\eta - 2v + 1)}{(\eta - 3)(\eta - v)}\right] \tag{A23}$$

where $\eta = \delta^{-1}_{N_2}$. This expression is for a linear quadrupole moment with a Morse oscillator (ref. 57) and it agrees very well with the results of Truhlar (ref. 58).

The variable parameters A_{st}, W_{st}, and K^{st}_{VV} were determined by curve-fitting equation (A19) to experimentally measured rate data for CO-CO and CO-N_2 V-V transitions. (See refs. 46, 52, and 59 to 66.) The values for these constants and for ℓ_{st} are given in table VII.

TABLE VII.- EMPIRICAL CONSTANTS FOR V-V RATE COEFFICIENTS

	A_{st}	W_{st}	K^{st}_{VV}	ℓ_{st}, Å
CO-CO	1.16681	64.155	3.06156×10^{-7}	0.203341
CO-N_2	1.42188	47.6964	6.954×10^{-8}	.20331
N_2-N_2	-------	-------	3.06156×10^{-7}	.20328

No experimental data were available for N_2-N_2 V-V transitions, but since CO and N_2 have the same molecular weight and very nearly equal vibrational energy level spacings, SSH theory (ref. 29) predicts that

$$K^{CO-CO}_{VV} \approx K^{N_2-N_2}_{VV} \tag{A24}$$

However, when this assumption was used, false inversions in the number densities for N_2 were obtained on the upper vibrational levels even when relatively large numbers of vibrational levels were carried in the calculations. Thus, this constant was decreased by a factor of 10. The values of ℓ_{CO-CO} and $\ell_{N_2-N_2}$ are taken from the V-T rate expressions and

$$\ell_{CO-N_2} = \sqrt{\ell_{CO-CO}\ell_{N_2-N_2}} \tag{A25}$$

This expression is based on the combining rule for Lennard-Jones potentials given in equation (A8) and simple SSH theory (ref. 29). The long-range quadrupole-quadrupole contribution to the N_2-N_2 V-V TP's was found to be negligible and was not used.

APPENDIX A

The V-V rate coefficients given by equation (A19) automatically satisfy detailed balancing, that is,

$$VV^{ss}_{v'+1,v-1} = VV^{ss}_{v,v'} \exp\left(-\frac{\theta^{ss}_{v,v'}}{T}\right) \tag{A26}$$

and

$$VV^{st}_{v'+1,v-1} = VV^{st}_{v,v'} \exp\left(-\frac{\theta^{st}_{v,v'}}{T}\right) \tag{A27}$$

Figures 14 to 18 show the theoretical VV rates for CO-CO, CO-N_2, and N_2-N_2 transitions together with the experimental data points used in obtaining the curve fits. In figure 14 the data of Wittig and Smith (ref. 59) was not used in the curve fitting because their experimental techniques have been questioned (ref. 60). In figure 17 the data from Sato et al. (ref. 61) and von Rosenberg et al. (ref. 62) were not used because of the large scatter in their results.

APPENDIX B

ELECTRON DISTRIBUTION FUNCTION AND EXCITATION RATES

To obtain the electron impact vibrational excitation and ionization rates which appear in the governing equations, an electron distribution function is obtained from a solution of the electron Boltzmann equation (refs. 28 and 67) and these rates are then calculated in terms of that function.

The electron Boltzmann equation used in this analysis is an adaptation of the one for electrons in a pure gas (ref. 68) and is derived under the assumption that the density of the gas is high enough to insure that the electron density gradients may be neglected (ref. 68). It can be written as

$$\frac{E^2}{3}\frac{d}{du}\left[\frac{u}{\sum_s (N_s Q_{sm})}\frac{df}{du}\right] + \sum_s \left[\frac{2m_e}{m_s}\frac{d}{du}\left(u^2 N_s Q_{sm} f\right)\right]$$

$$+ \sum_s \left[\frac{2m_e}{m_s}\frac{kT}{e}\frac{d}{du}\left(u^2 N_s Q_{sm}\frac{df}{du}\right)\right] + \sum_s N_s\left\{\sum_J \left[(u + u_{sJ})\, f(u + u_{sJ})\, Q_{sJ}(u + u_{sJ})\right]\right.$$

$$- u\, f(u) \sum_J \left[Q_{sJ}(u)\right] + \sum_J \left[(u - u_{sJ})\, f(u - u_{sJ})\, Q^*_{sJ}(u - u_{sJ})\right]$$

$$\left. - u\, f(u) \sum_J \left[Q^*_{sJ}(u)\right]\right\} = 0 \qquad \text{(B1)}$$

This is a difference-differential equation which requires a numerical solution technique. To facilitate the solution, Phelps and his associates (refs. 68 and 69) have developed approximations for the large number of inelastic rotational terms in this equation which are valid when the average electron energy is much greater than the gas temperature. This simplification is extremely important since, in order to obtain an accurate solution of equation (B1), the energy difference between mesh points must be taken smaller than any of the u_{sJ}. For CO, the extremely large number of mesh points that would be required would make a solution of the equation impractical. When rotational excitation is dominated by the electric dipole moment as in CO, the rotational inelastic terms can be approximated by (ref. 68)

$$N_s K_{sD} \frac{d}{du}\left[u^{1/4} f(u)\right] \qquad \text{(B2)}$$

where

$$\left.\begin{aligned} K_{sD} &= \Gamma\left(\frac{15}{8}\right)(2)^{7/4} R_\infty (B_{s0})^{7/8} \left(\frac{kT}{e}\right)^{-1/8} \sigma_{sD} \\ \sigma_{sD} &= \frac{8\pi}{3} a_0^2 \theta_{sD}^2 \end{aligned}\right\} \tag{B3}$$

For N_2, where these processes are dominated by the electric quadrupole moment, the rotational inelastic terms are approximated by

$$N_s K_{sQ} \frac{d}{du}\left[u\, f(u)\right] \tag{B4}$$

where

$$\left.\begin{aligned} K_{sQ} &= 4 B_{s0} \sigma_{sQ} \\ \sigma_{sQ} &= \frac{8\pi}{15} a_0 \theta_{sQ}^2 \end{aligned}\right\} \tag{B5}$$

In addition, it is assumed that the populations of excited states are much smaller than that of the ground state. Thus, the last two terms of equation (B1) can be neglected. With all these approximations, equation (B1) becomes

$$\frac{d}{du}\left[A(u)\frac{df}{du} + B(u)\, f\right] - C(u)\, f + D(u) = 0 \tag{B6}$$

where

$$\left.\begin{aligned} A(u) &= \frac{u}{3Q_1}\left(\frac{E}{N}\right)^2 + \lambda u_T Q_2 u^2 \\ B(u) &= \lambda Q_2 u^2 + K_D u^{1/4} + K_Q u \\ C(u) &= u \sum_s \beta_s \sum_J Q_{sJ}(u) \\ D(u) &= \sum_s \beta_s \sum_J \left(u + u_{sJ}\right) f\left(u + u_{sJ}\right) Q_{sJ}\left(u + u_{sJ}\right) \end{aligned}\right\} \tag{B7}$$

and

$$\left.\begin{aligned}
\beta_s &= \frac{N_s}{N} \\
Q_1 &= \sum_s \beta_s Q_{sm} \\
M &= \sum_s \beta_s m_s \\
Q_2 &= \sum_s \beta_s Q_{sm} \frac{M}{m_s} \\
K_D &= \sum_s \beta_s K_{sD} \\
K_Q &= \sum_s \beta_s K_{sQ} \\
\lambda &= \frac{2m_e}{M} \\
u_T &= \frac{kT}{e}
\end{aligned}\right\} \qquad \text{(B8)}$$

All the momentum, vibrational, and electronic excitation cross sections and the ionization cross sections which appear in equation (B6), except those for the electronic excitation of CO, can be found in tabulated form in reference 69. The CO electronic cross sections are calculated from the semiempirical formulas of Sawada et al. (ref. 70).

To facilitate the integration of equation (B6), it can be written as two first-order differential equations

$$\frac{df}{du} = \frac{g(u) - B(u)\, f(u)}{A(u)} \qquad \text{(B9)}$$

$$\frac{dg}{du} = C(u)\, f(u) - D(u) \qquad \text{(B10)}$$

where

$$g(u) = A(u)\frac{df}{du} + B(u)\, f(u) \qquad \text{(B11)}$$

APPENDIX B

The initial conditions on f and g are

$$\left.\begin{aligned} f(u_{max}) &= f_0 > 0 \\ g(u_{max}) &= 0 \end{aligned}\right\} \tag{B12}$$

where f_0 is a very small constant (-10^{-30}). The value of u_{max} is chosen large enough to insure that f(u) can be assumed to be essentially equal to zero for $u > u_{max}$. Equations (B9) and (B10) are integrated backward from $u = u_{max}$ to $u = 0$ by using a constant-step-size, fourth-order Adams-Moulton predictor-corrector method. The step-size value is dependent on the E/N value. The solution for f(u) is normalized so that

$$\int_0^\infty u^{1/2} f(u)\, du = 1 \tag{B13}$$

As a check on the accuracy of the solution for f(u), the electron energy equation is calculated as well. This equation is obtained by multiplying equation (B6) by $\left(\frac{2e}{m_e}\right)^{1/2} u\, du$ and integrating it over all energies (ref. 68) and it is a statement of the fact that the power input to the electrons from the electric field must be exactly balanced by the power losses of the electrons from elastic and inelastic collisions. It can be written

$$\begin{aligned} w\frac{E}{N} = {} & \sqrt{\frac{2e}{m_e}}\left(\frac{2m_e}{M}\right)\int_0^\infty u^2 Q_2(u)\, f(u)\, du + \sqrt{\frac{2e}{m_e}}\left(\frac{2m_e}{M}\right)\left(\frac{kT}{e}\right)\int_0^\infty u^2 Q_2(u)\frac{df}{du}\, du \\ & + \sqrt{\frac{2e}{m_e}}\, K_D \int_0^\infty u^{1/4} f(u)\, du + \sqrt{\frac{2e}{m_e}}\, K_Q \int_0^\infty u\, f(u)\, du \\ & + \sqrt{\frac{2e}{m_e}} \sum_s \left[\beta_s \sum_J u_{sJ} \int_0^\infty u\, Q_{sJ}(u)\, f(u)\, du\right] \end{aligned} \tag{B14}$$

where

$$w = (\mu N)\frac{E}{N} \tag{B15}$$

and

$$\mu N = -\frac{1}{3}\sqrt{\frac{2e}{m_e}} \int_0^\infty \frac{u}{Q_1(u)}\frac{df}{du}\, du \tag{B16}$$

If the left and right sides of equation (B14) differ by more than 1 percent, the integration for f(u) is repeated with a smaller step size. The electron temperature is given by

$$T_e = \frac{2}{3}\frac{e}{k}\int_0^\infty u^{3/2} f(u)\, du \tag{B17}$$

Thus, for a given E/N and a given composition, an electron temperature can be determined from the distribution function solution. By obtaining solutions for several E/N values for a given composition, a table of electron temperatures for various E/N values can be constructed. Interpolation in this table gives the proper electron temperature value for the conditions in the laser cavity.

The current density can be related to the electron drift velocity by

$$j = eN_e w \tag{B18}$$

or

$$j = eN_e \mu N \frac{E}{N} \tag{B19}$$

Equation (B19) can be used to calculate the electron number density for the given set of conditions under consideration.

The rate for electron impact excitation from the vibrational ground state can be written as

$$P_{0v}^s = \sqrt{\frac{2e}{m_e}}\int_0^\infty u Q_{sv}(u) f(u)\, du \tag{B20}$$

The rate for electron impact deexcitation from vibrational state v to the ground state is

$$P_{v0}^s = \sqrt{\frac{2e}{m_e}}\int_0^\infty u Q_{sv}^*(u) f(u)\, du \tag{B21}$$

where the principle of microscopic reversibility is used to obtain Q_{sv}^* from

$$uQ_{sv}^*(u) = (u + u_{sv})Q_{sv}(u + u_{sv}) \tag{B22}$$

Results of distribution function calculations for two gas mixtures are presented in figures 19 to 21. Figure 19 shows the variation of P_{0v}^{CO} (for v = 1, 4, and 8) with E/N for the case

$$\left.\begin{aligned} \dot{m}_{CO} &= 1.96 \times 10^{-5} \text{ g/sec} \\ \dot{m}_{He} &= 3.91 \times 10^{-4} \text{ g/sec} \end{aligned}\right\} \tag{B23}$$

and figure 20 shows the same results for the case

$$\left.\begin{aligned} \dot{m}_{CO} &= 1.92 \times 10^{-5} \text{ g/sec} \\ \dot{m}_{N_2} &= 3.81 \times 10^{-5} \text{ g/sec} \\ \dot{m}_{He} &= 3.83 \times 10^{-4} \text{ g/sec} \end{aligned}\right\} \tag{B24}$$

Figure 21 shows the variation of electron temperature with E/N for the same two cases. The constants which appear in equations (B2) to (B5) are

$$\left.\begin{aligned} B_{CO,0} &= 2.4 \times 10^{-4} \text{ eV} \\ \theta_{CO,D} &= 4.6 \times 10^{-2} \text{ ea}_0^{(66)} \\ B_{N_2,0} &= 2.5 \times 10^{-4} \text{ eV} \\ \theta_{N_2,Q} &= 1.04 \text{ ea}_0^{2(67)} \\ a_0 &= 5.29 \times 10^{-9} \text{ cm} \\ R_\infty &= 13.6 \text{ eV} \end{aligned}\right\} \tag{B25}$$

APPENDIX C

GAIN COEFFICIENT

The expression used in this analysis for the gain coefficient for a given P(J) branch transition where the rotational quantum number changes from J - 1 to J as the vibrational quantum number changes from v to v - 1 is due to Lacina (ref. 7). It is given by

$$\gamma_{v,J} = \frac{A_1^{(1)} c^2 \nu_{v,J}}{8\pi\nu_1^3 kT} JS_v \left| \frac{R_{v,v-1}^{CO}}{R_{1,0}^{CO}} \right|^2 \left\{ N_{CO,v} B_v \exp\left[-\frac{hc}{kT} B_v J(J-1) \right] \right.$$

$$\left. - N_{CO,v-1} B_{v-1} \exp\left[-\frac{hc}{kT} B_{v-1} J(J+1) \right] \right\} \tag{C1}$$

where

$$\nu_v = c\left[G_{CO}(v) - G_{CO}(v-1) \right] \tag{C2}$$

The expression for $G_{CO}(v)$ is given by equations (16) and the values of $A_1^{(1)}$ and $\left| R_{v,v-1}^{CO} / R_{1,0}^{CO} \right|^2$ are given in table I.

The derivation of equation (C1) assumes that the rotational levels are in equilibrium at the given gas temperature. The effects of both Doppler and pressure broadening (ref. 7) are included in the expression for the line shape factor

$$S_v = \frac{1}{\sqrt{\pi}\Delta\nu_D} \exp(x^2) \operatorname{erfc}(x) \tag{C3}$$

where

$$x = \frac{\Delta\nu_c}{\Delta\nu_D} \tag{C4a}$$

$$\Delta\nu_D = \left(\frac{2kT}{m_{CO}} \right)^{1/2} \nu_v \tag{C4b}$$

$$\Delta\nu_c = \frac{f_c}{2\pi} \tag{C4c}$$

and (ref. 68)

$$f_c = \sum_s N_s \sigma_{opt}^{CO,s} \left(\frac{2kT}{\mu_{CO,s}} \right)^{1/2} \tag{C4d}$$

APPENDIX C

The optical cross sections are taken from Williams et al. (ref. 24)

$$\left.\begin{aligned} \sigma_{opt}^{CO\text{-}CO} &= 8.0 \times 10^{-15}\ cm^2 \\ \sigma_{opt}^{CO\text{-}N_2} &= 7.35 \times 10^{-15}\ cm^2 \\ \sigma_{opt}^{CO\text{-}He} &= 3.0 \times 10^{-15}\ cm^2 \end{aligned}\right\} \tag{C5}$$

These cross sections decrease with increasing rotational quantum number J. Equations (C5) give values corresponding to J = 11.

The frequency for a given P(J) transition is given by

$$\nu_{v,J} = c\left[G_{CO}(v) - G_{CO}(v - 1) + F_v(J - 1) - F_{v-1}(J)\right] \tag{C6}$$

where

$$F_v(J) = B_v J(J + 1) - D_v J^2(J + 1)^2 \tag{C7}$$

and

$$B_v = 1.93141 - 0.01752\left(v + \frac{1}{2}\right) + 2.96 \times 10^{-6}\left(v + \frac{1}{2}\right)^2 \tag{C8}$$

$$D_v = 6.18 \times 10^{-6} - 1.76 \times 10^{-9}\left(v + \frac{1}{2}\right) \tag{C9}$$

The units of F_v, B_v, and D_v are cm^{-1}. The constants in equations (C8) and (C9) are taken from Patel. (See ref. 15.)

REFERENCES

1. McClatchey, R. A.: Atmospheric Attenuation of CO Laser Radiation. AFCRL-71-0370 (Environ. Res. Paper No. 359), U.S. Air Force, July 1971. (Available from DDC as AD 729 447.)

2. Bhaumik, Mani L.; Lacina, W. B.; and Mann, Michael M.: Characteristics of a CO Laser. IEEE J. Quant. Electr., vol. QE-8, no. 2, Feb. 1972, pp. 150-160.

3. Djeu, N.: Energy Exchange Processes in a Low Temperature N_2-CO Transfer Laser. Chem. Phys. Lett., vol. 15, no. 3, Aug. 1972, pp. 392-395.

4. Djeu, N.: CW Single-Line CO Laser on the $v = 1 \rightarrow v = 0$ Band. Appl. Phys. Lett., vol. 23, no. 6, Sept. 1973, pp. 309-310.

5. Smith, Neill S.; and Hassan, H. A.: Power Calculations for High-Flow CO Electric Discharge Laser Systems. AIAA Paper No. 75-35, Jan. 1975.

6. Rich, Joseph W.: Kinetic Modeling of the High-Power Carbon Monoxide Laser. J. Appl. Phys., vol. 42, no. 7, June 1971, pp. 2719-2730.

7. Lacina, W. B.: Kinetic Model and Theoretical Calculations for Steady State Analysis of Electrically Excited CO Laser Amplifier System Final Report: Part II. NCL 71-32R (Contract N00014-71-C-0037), U.S. Navy, Aug. 1971. (Available from DDC as AD 729 235.)

8. Center, R. E.; and Caledonia, G. E.: Theoretical Description of the Electrical CO Laser. Appl. Phys. Lett., vol. 19, no. 7, Oct. 1971, pp. 211-213.

9. Sidney, B.; McInville, Roy M.; and Hassan, H. A.: Theory and Experiment of Low Transitions in CO Discharge Lasers. AIAA Paper No. 75-850, June 1975.

10. Boness, M. J. W.; and Schulz, G. J.: Excitation of High Vibrational States of N_2 and CO via Shape Resonances. Phys. Rev., vol. 8, no. 6, Dec. 1973, pp. 2883-2886.

11. Lordi, J. A.; Falk, T. J.; and Rich, J. W.: Analytical Studies of the Kinetics of Electrically Excited, Continuously Operating CO Flow Lasers. AIAA Paper No. 74-563, June 1974.

12. Chen, Joseph C. Y.: Theory of Subexcitation Electron Scattering by Molecules. II. Excitation and De-Excitation of Molecular Vibration. J. Chem. Phys., vol. 40, no. 12, June 15, 1964, pp. 3513-3520.

13. Abraham, George; and Fisher, Edward R.: Modeling of a Pulsed CO/N_2 Molecular Laser System. J. Appl. Phys., vol. 43, no. 11, Nov. 1972, pp. 4621-4631.

14. Young, Lee A.; and Eachus, W. James: Dipole Moment Function and Vibration-Rotation Matrix Elements for CO. Chem. Phys., vol. 44, no. 11, June 1, 1966, pp. 4195-4206.

15. Patel, C. K. N.: CW Laser on Vibrational-Rotational Transitions of CO. Appl. Phys. Lett., vol. 7, no. 9, Nov. 1965, pp. 246-247.

16. Herzberg, Gerhard: Molecular Spectra and Molecular Structure. I. Spectra of Diatomic Molecules. Second ed., D. Van Nostrand Co., Inc., c.1950.

17. Vasil'ev, S. S.; and Sergeenkova, E. D.: Energetic Calculation and Spectroscopic Determination of Molecular Temperatures at Moderate Pressures in the Electric Discharge Zone. Russian J. Phys. Chem., vol. 40, no. 10, Oct. 1966, pp. 1277-1299.

18. Eckert, E. R. G.; and Drake, Robert M., Jr.: Heat and Mass Transfer. Second ed., McGraw-Hill Book Co., Inc., 1959.

19. Touloukian, Y. S.; Liley, P. E.; and Saxena, S. C.: Thermal Conductivity – Nonmetallic Liquids and Gases. Thermophysical Properties of Matter, Vol. 3, Y. S. Touloukian and C. Y. Ho, eds., IFI Plenum, c.1970.

20. Cool, Terrill A.: Power and Gain Characteristics of High Speed Flow Lasers. J. Appl. Phys., vol. 40, no. 9, Aug. 1969, pp. 3563-3573.

21. Nighan, William L.: Electron Kinetic Processes in CO Lasers. Appl. Phys. Lett., vol. 20, no. 2, Jan. 1972, pp. 96-99.

22. Greene, A. E.; and Harris, R. A.: Temperature Dependence for Carbon Monoxide Optical Broadening Cross Sections. J. Appl. Phys., vol. 46, no. 11, Nov. 1975, p. 5039.

23. Varanasi, Prasad: Measurement of Line Widths of CO of Planetary Interest at Low Temperatures. J. Quant. Spectrosc. Radiat. Transfer, vol. 15, no. 2, Feb. 1975, pp. 191-196.

24. Williams, Dudley; Wenstrand, David C.; Brockman, Robert J.; and Curnutte, Basil: Collisional Broadening of Infra-Red Absorption Lines. Molecular Phys., vol. 20, no. 5, May 1971, pp. 769-785.

25. Keren, H.; Avivi, P.; and Dothan, F.: The Influence of Oxygen on CO-Laser Performance. IEEE J. Quant. Electr., vol. QE-11, no. 8, Aug. 1975, pp. 590-594.

26. Cross, Peter S.; and Oldham, William G.: Theory of Optical-Gain Measurements. IEEE J. Quant. Electr., vol. QE-11, no. 5, May 1975, pp. 190-197.

27. Nighan, William L.; and Wiegand, W. J.: Influence of Negative-Ion Processes on Steady-State Properties and Striations in Molecular Gas Discharges. Phys. Rev., vol. 10, no. 3, Sept. 1974, pp. 922-945.

28. Nighan, William L.: Stability of High Power Molecular Laser Discharges. UTR75-19, United Technol. Res. Center, May 1975.

29. Herzfeld, Karl F.; and Litovitz, Theodore A.: Absorption and Dispersion of Ultrasonic Waves. Academic Press, Inc., 1959.

30. Keck, James; and Carrier, George: Diffusion Theory of Nonequilibrium Dissociation and Recombination. J. Chem. Phys., vol. 43, no. 7, Oct. 1, 1965, pp. 2284-2298.

31. Bray, K. N. C.: Vibrational Relaxation of Anharmonic Oscillator Molecules: Relaxation Under Isothermal Conditions. J. Phys. B (Proc. Phys. Soc.), ser. 2, vol. 1, no. 4, July 1968, pp. 705-717.

32. Shin, Hyung Kyu: Dependence of the Probabilities of Vibrational De-Excitation on Interaction Potentials. J. Chem. Phys., vol. 42, no. 1, Jan. 1, 1965, pp. 59-62.

33. Thompson, Samuel L.: Vibration-Translational Energy Transfer According to the Morse Potential. J. Chem. Phys., vol. 49, no. 8, Oct. 15, 1968, pp. 3400-3410.

34. Hirschfelder, Joseph O.; Curtiss, Charles F.; and Bird, R. Byron: Molecular Theory of Gases and Liquids. John Wiley & Sons, Inc., 1964.

35. Good, Robert J.; and Hope, Christopher J.: New Combining Rule for Intermolecular Distances in Intermolecular Potential Function. J. Chem. Phys., vol. 53, no. 2, July 15, 1970, pp. 540-543.

36. Good, Robert J.; and Hope, Christopher J.: Test of Combining Rules for Intermolecular Distances. Potential Function Constants From Second Virial Coefficients. J. Chem. Phys., vol. 55, no. 1, July 1, 1971, pp. 111-116.

37. Neufeld, Philip D.; Janzen, A. R.; and Aziz, R. A.: Empirical Equations To Calculate 16 of the Transport Collision Integrals $\Omega(\ell,s)^*$ for the Lennard-Jones (12-6) Potential. J. Chem. Phys., vol. 57, no. 3, Aug. 1, 1972, pp. 1100-1102.

38. Kieffer, L. J.: A Compilation of Electron Collision Cross Section Data for Modeling Gas Discharge Lasers. JILA-IC-13, Joint Inst. Lab. Astrophys., Sept. 1973.

39. Shin, Hyung Kyu: Vibrational Relaxation in CO + He at Low Temperatures. J. Chem. Phys., vol. 55, no. 11, Dec. 1, 1971, pp. 5233-5234.

40. Miller, Donald J.; and Millikan, Roger C.: Vibrational Relaxation of Carbon Monoxide by Hydrogen and Helium Down to 100° K. J. Chem. Phys., vol. 53, no. 8, Oct. 15, 1970, pp. 3384-3385.

41. Hooker, William J.; and Millikan, Roger C.: Shock-Tube Study of Vibrational Relaxation in Carbon Monoxide for the Fundamental and First Overtone. J. Chem. Phys., vol. 38, no. 1, Jan. 1, 1963, pp. 214-220.

42. Millikan, Roger C.: Carbon Monoxide Vibrational Relaxation in Mixtures With Helium, Neon, and Krypton. J. Chem. Phys., vol. 40, no. 9, May 1, 1964, pp. 2594-2596.

43. Millikan, Roger C.; and White, Donald R.: Vibrational Energy Exchange Between N_2 and CO. The Vibrational Relaxation of Nitrogen. J. Chem. Phys., vol. 39, no. 1, July 1, 1963, pp. 98-101.

44. Kovacs, M. A.: VT Relaxation in N_2 and CO. IEEE J. Quant. Electr., vol. QE-9, no. 1, Jan. 1973, p. 189.

45. Millikan, Roger C.: Vibrational Fluorescence of Carbon Monoxide. J. Chem. Phys., vol. 38, no. 12, June 15, 1963, pp. 2855-2860.

46. Green, W. H.; and Hancock, J. K.: Measurement of CO (v = 1) Vibrational Energy Transfer Rates Using a Frequency-Doubled CO_2 Laser. J. Chem. Phys., vol. 59, no. 8, Oct. 15, 1973, pp. 4326-4335.

47. White, Donald R.: Vibrational Relaxation of Shocked N_2-He, N_2-CH_4, and N_2-C_2H_2 Mixtures. J. Chem. Phys., vol. 48, no. 1, Jan. 1, 1968, pp. 525-526.

48. Jeffers, W. Q.; and Kelley, J. Daniel: Calculations of V-V Transfer Probabilities in CO-CO Collisions. J. Chem. Phys., vol. 55, no. 9, Nov. 1, 1971, pp. 4433-4437.

49. Sharma, R. D.; and Brau, C. A.: Energy Transfer in Near-Resonant Molecular Collisions Due to Long-Range Forces With Application to Transfer of Vibrational Energy From ν_3 Mode of CO_2 to N_2. J. Chem. Phys., vol. 50, no. 2, Jan. 15, 1969, pp. 924-929.

50. Caledonia, G. E.; and Center, R. E.: Vibrational Distribution Functions in Anharmonic Oscillators. J. Chem. Phys., vol. 55, no. 2, July 15, 1971, pp. 552-561.

51. Rapp, Donald; and Englander-Golden, P.: Resonant and Near-Resonant Vibrational-Vibrational Energy Transfer Between Molecules in Collisions. J. Chem. Phys., vol. 40, no. 2, Jan. 15, 1964, pp. 573-575.

52. Hancock, G.; and Smith, I. W. M.: Quenching of Infrared Chemiluminescence. 1: The Rates of De-Excitation of CO ($4 \leq v \leq 13$) by He, CO, NO, N_2, O_2, OCS, N_2O, and CO_2. Appl. Optics, vol. 10, no. 8, Aug. 1971, pp. 1827-1842.

53. Dillon, T. A.; and Stephenson, J. C.: Multiquantum Vibrational-Energy Exchange. Phys. Rev., vol. 6, no. 4, Oct. 1972, pp. 1460-1468.

54. Dillon, T. A.; and Stephenson, J. C.: Effect of the Straight Path Approximation and Exchange Forces on Vibrational Energy Transfer. J. Chem. Phys., vol. 58, no. 9, May 1, 1973, pp. 3849-3854.

55. Rockwood, Stephen D.; Brau, James E.; Proctor, William A.; and Canavan, Gregory H.: TA9-Time-Dependent Calculations of Carbon Monoxide Laser Kinetics. IEEE J. Quant. Electr., vol. QE-9, no. 1, Jan. 1973, pp. 120-129.

56. Plummer, Michael J.; and Glowacki, Walter J.: Theoretical Investigation of the CO Supersonic Electric Discharge Laser. AIAA Paper No. 73-623, July 1973.

57. Heaps, H. S.; and Herzberg, G.: Intensity Distribution in the Rotation-Vibration Spectrum of the OH Molecule. Zeitschr. für Phys., Bd. 133, Heft 1, Sept. 1952, pp. 48-64.

58. Truhlar, Donald G.: Vibrational Matrix Elements of the Quadrupole Moment Functions of H_2, N_2 and CO. Internat. J. Quant. Chem., vol. VI, no. 5, Sept. 1972, pp. 975-988.

59. Wittig, Curt; and Smith, Ian W. M.: Vibrational Relaxation of Carbon Monoxide ($4 \leq v \leq 10$) at $T \approx 100^{\circ}$ K. Chem. Phys. Lett., vol. 16, no. 2, Oct. 1972, pp. 292-295.

60. Jeffers, William Q.; and Powell, Howard T.: Carbon Monosulfide and CO Probe Laser Research – Final Report. MDC Q0498 (Contract N00014-72-C-0458), U.S. Navy, July 31, 1973. (Available from DDC as AD 777 960.)

61. Sato, Yukinori; Tsuchiya, Soji; and Kuratani, Kenji: Shock-Wave Study of Vibrational Energy Exchange Between Diatomic Molecules. J. Chem. Phys., vol. 50, no. 5, Mar. 1, 1969, pp. 1911-1919.

62. Von Rosenberg, C. W., Jr.; Bray, K. N. C.; and Pratt, N. H.: Shock Tube Vibrational Relaxation Measurements: N_2 Relaxation by H_2O and the CO-N_2 V-V Rate. J. Chem. Phys., vol. 56, no. 7, Apr. 1, 1972, pp. 3230-3237.

63. Powell, H. T.: Vibrational Relaxation of Carbon Monoxide Using a Pulsed Discharge. J. Chem. Phys., vol. 59, no. 9, Nov. 1, 1973, pp. 4937-4941.

64. Stephenson, John C.: Vibrational Excitation and Relaxation of the CO ($v = 1$) and CO ($v = 2$) States. Appl. Phys. Lett., vol. 22, no. 11, June 1973, pp. 576-578.

65. Stephenson, John C.; and Mosburg, Earl R., Jr.: Vibrational Energy Transfer in CO From 100 to 300° K. J. Chem. Phys., vol. 60, no. 9, May 1, 1974, pp. 3562-3566.

66. Zittel, Paul F.; and Moore, C. Bradley: Vibration-to-Vibration Energy Transfer in N_2-CO. Appl. Phys. Lett., vol. 21, no. 3, Aug. 1972, pp. 81-83.

67. Nighan, William L.: Electron Energy Distributions and Collision Rates in Electrically Excited N_2, CO, and CO_2. Phys. Rev., vol. 2, no. 5, Nov. 1970, pp. 1989-2000.

68. Frost, L. S.; and Phelps, A. V.: Rotational Excitation and Momentum Transfer Cross Sections for Electrons in H_2 and N_2 From Transport Coefficients. Phys. Rev., vol. 127, no. 5, Sept. 1962, pp. 1621-1633.

69. Hake, R. D., Jr.; and Phelps, A. V.: Momentum-Transfer and Inelastic-Collision Cross Sections for Electrons in O_2, CO, CO_2. Phys. Rev., vol. 158, no. 1, June 1967, pp. 70-84.

70. Sawada, T.; Sellin, D. L.; and Green, A. E. S.: Electron Impact Excitation Cross Sections and Energy Degradation in CO. J. Geophys. Res., vol. 77, no. 25, Sept. 1972, pp. 4819-4828.

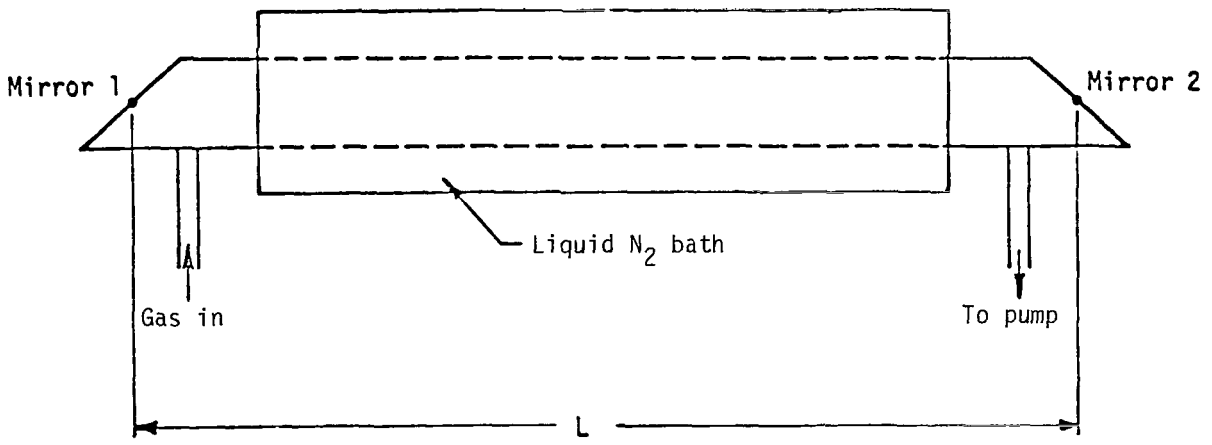

Figure 1.- Schematic of slow-flow electric discharge laser.

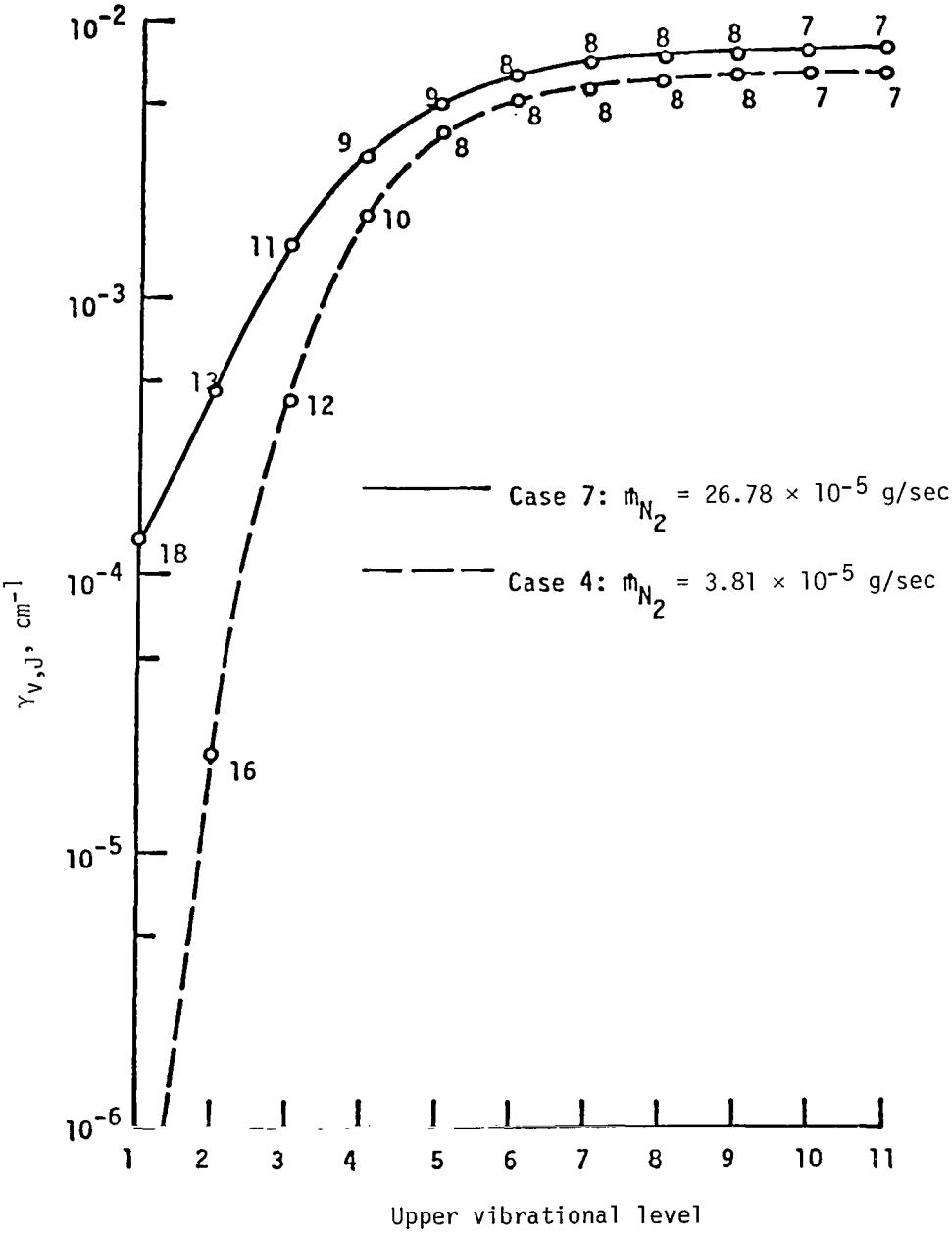

Figure 2.- Influence of N_2 fraction on maximum small signal gain coefficient.

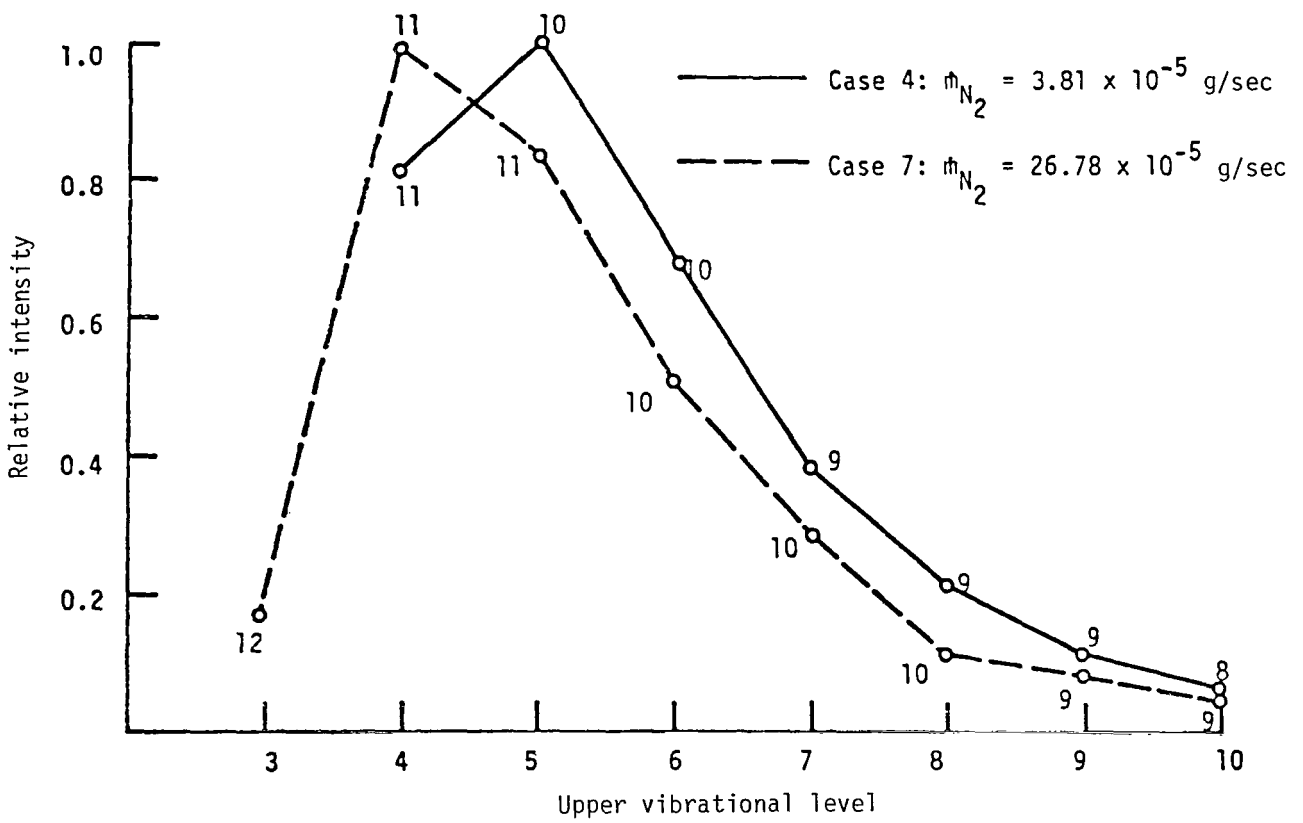

Figure 3.- Influence of N_2 fraction on relative lasing intensities.

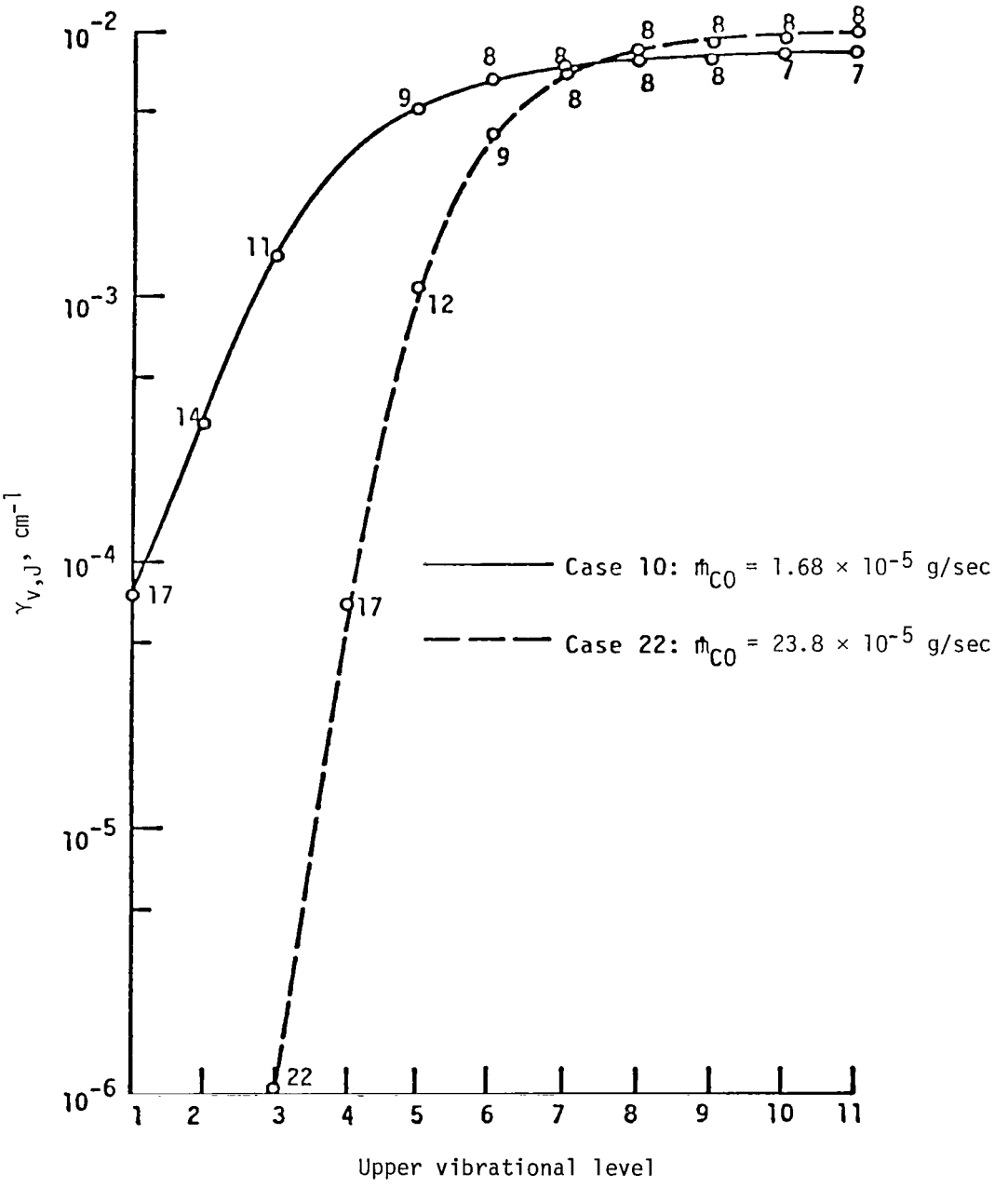

Figure 4.- Influence of CO fraction on maximum small signal gain coefficient.

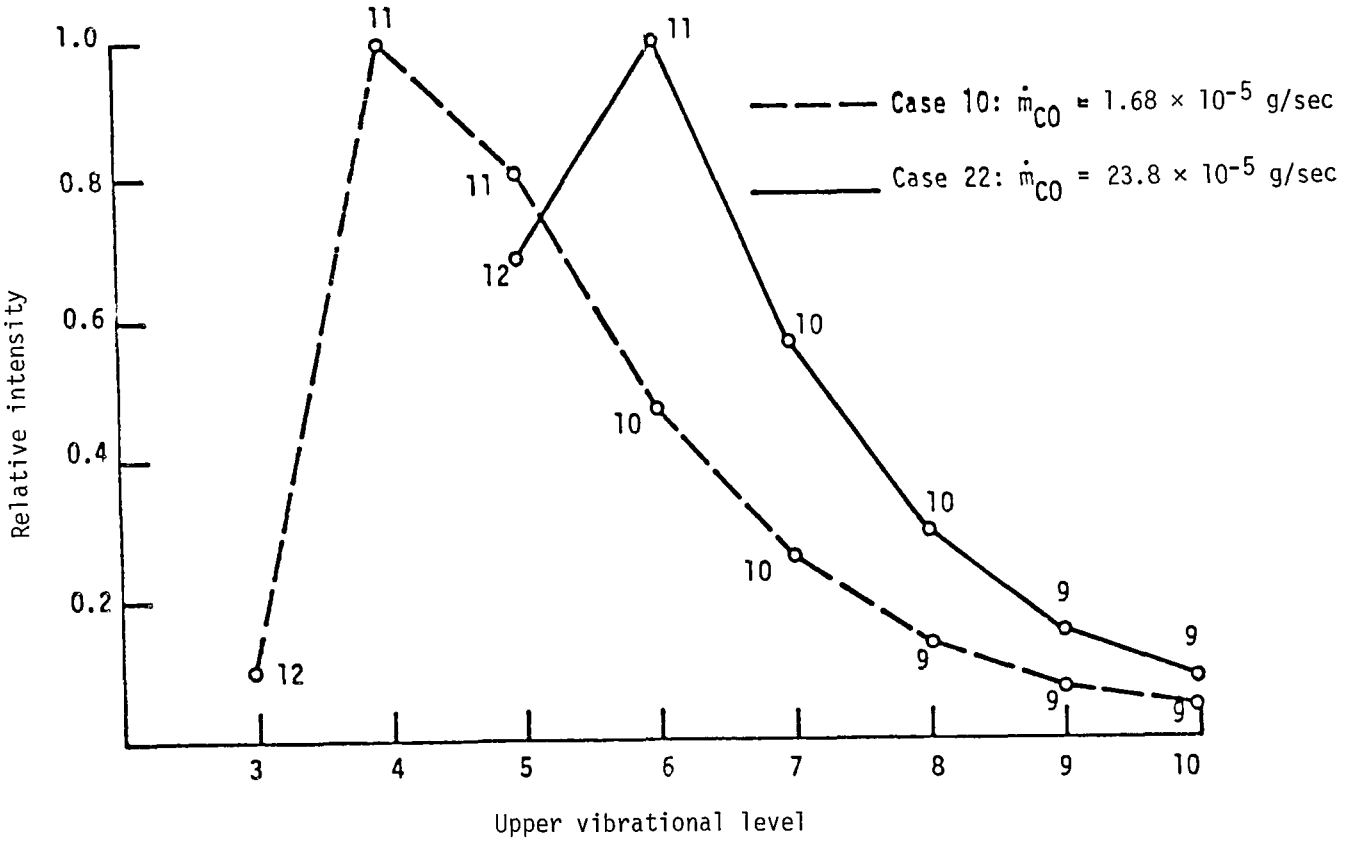

Figure 5.- Influence of CO fraction on relative lasing intensities.

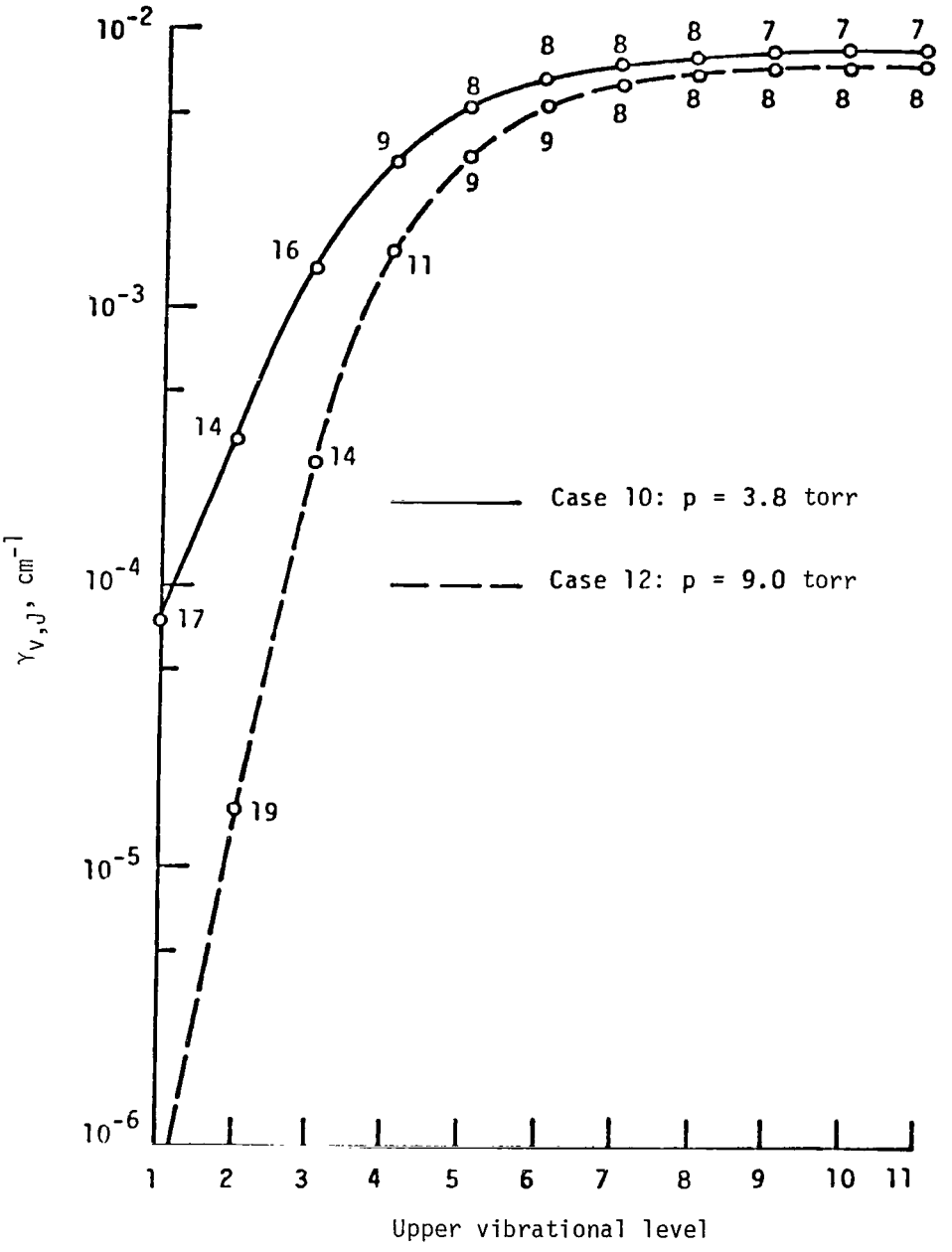

Figure 6.- Effect of pressure on maximum small signal gain coefficient.

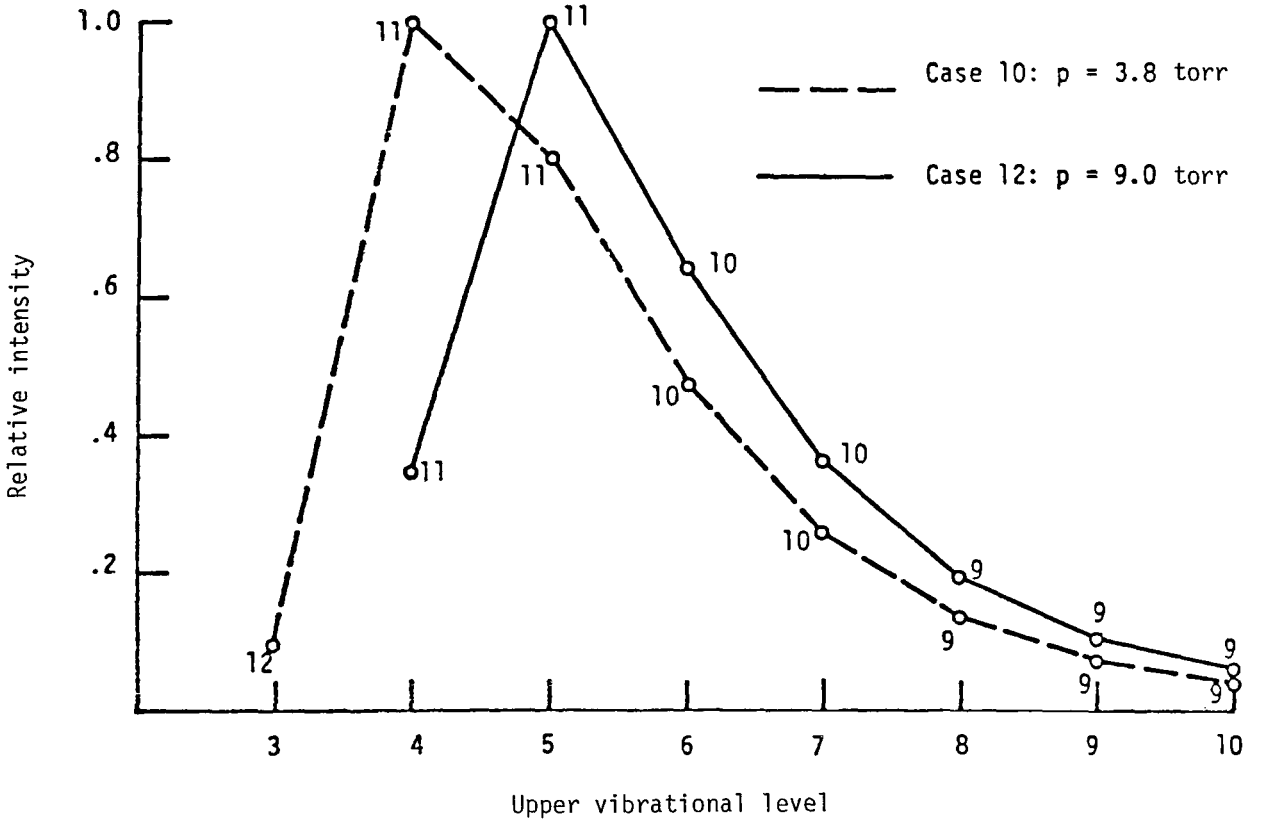

Figure 7.- Effect of pressure on relative lasing intensities.

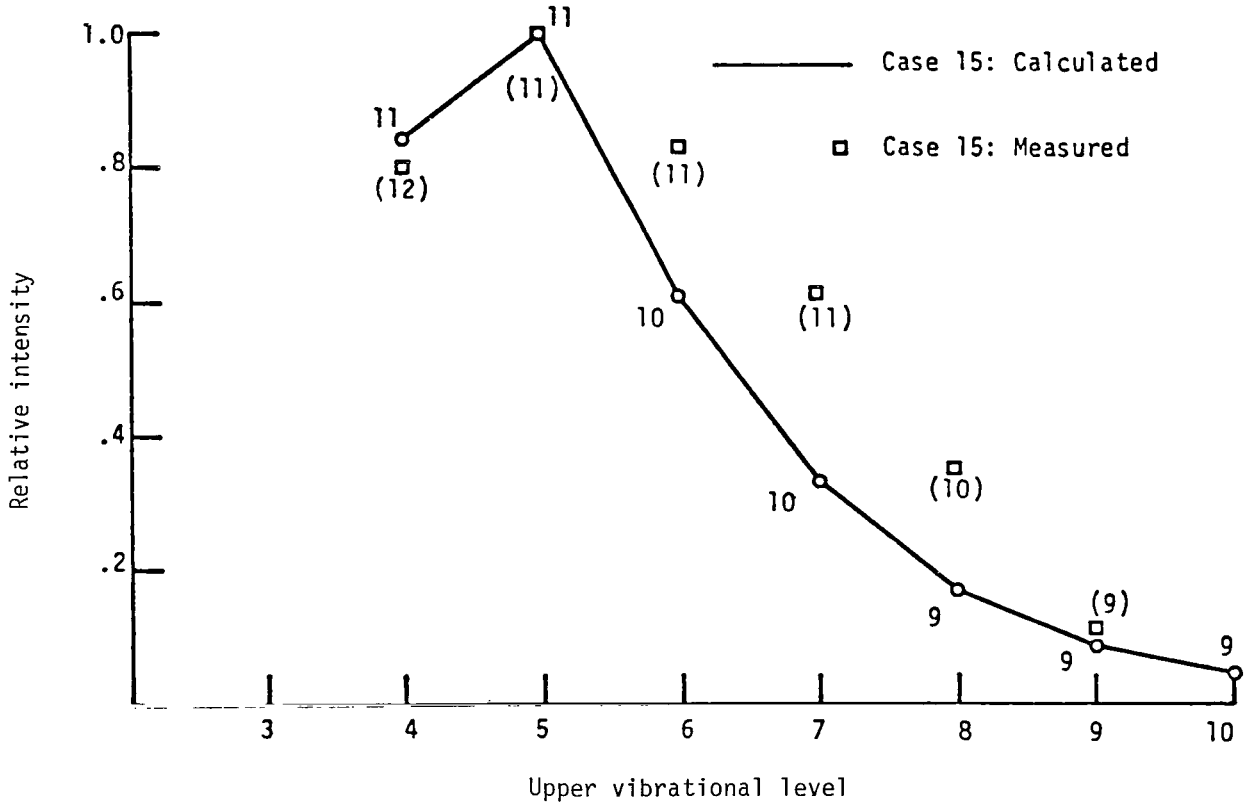

Figure 8.- Comparison of calculated and measured relative intensities.

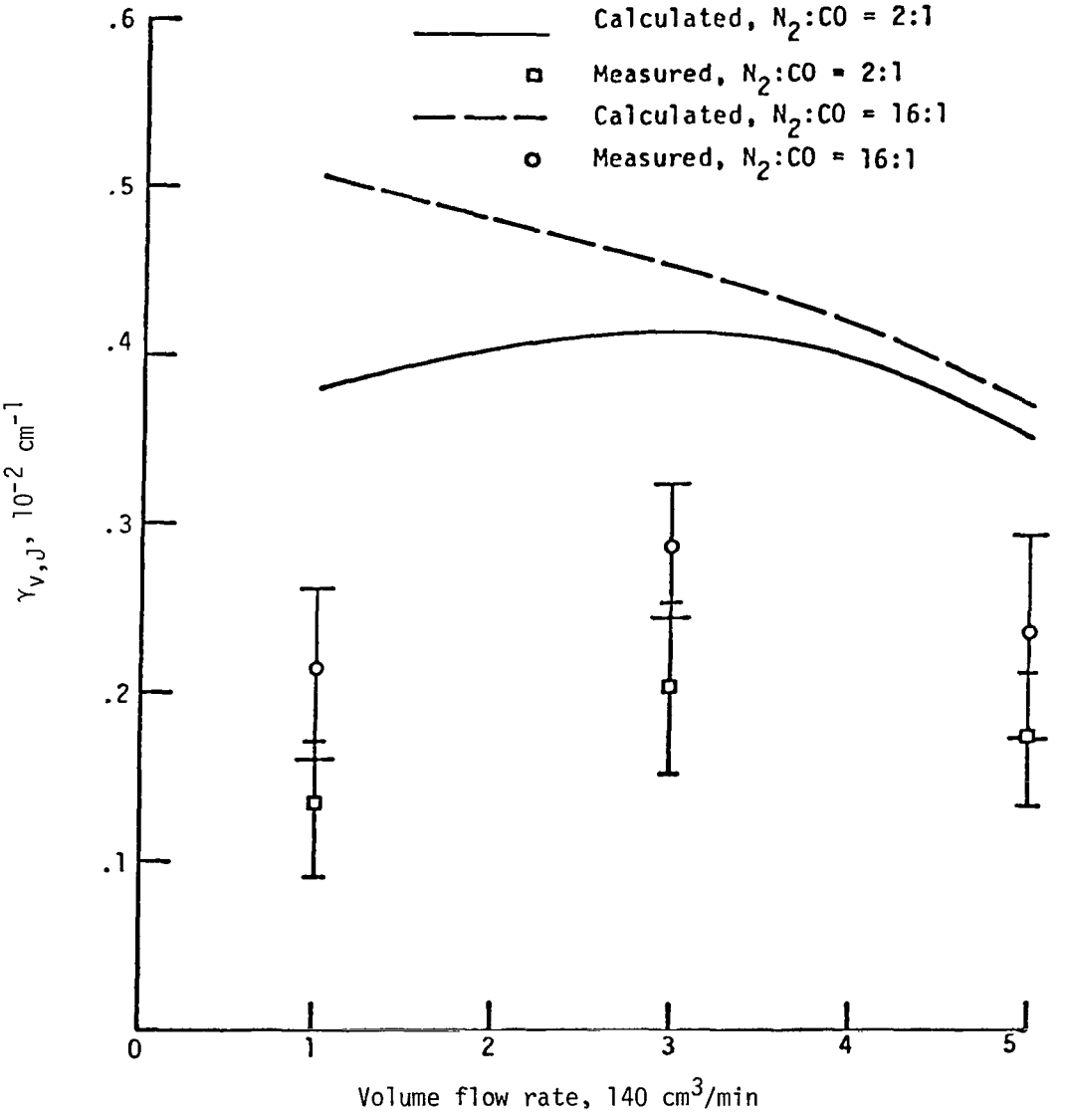

Figure 9.- Comparison of calculated and measured gain coefficients for 5→4(9) line.

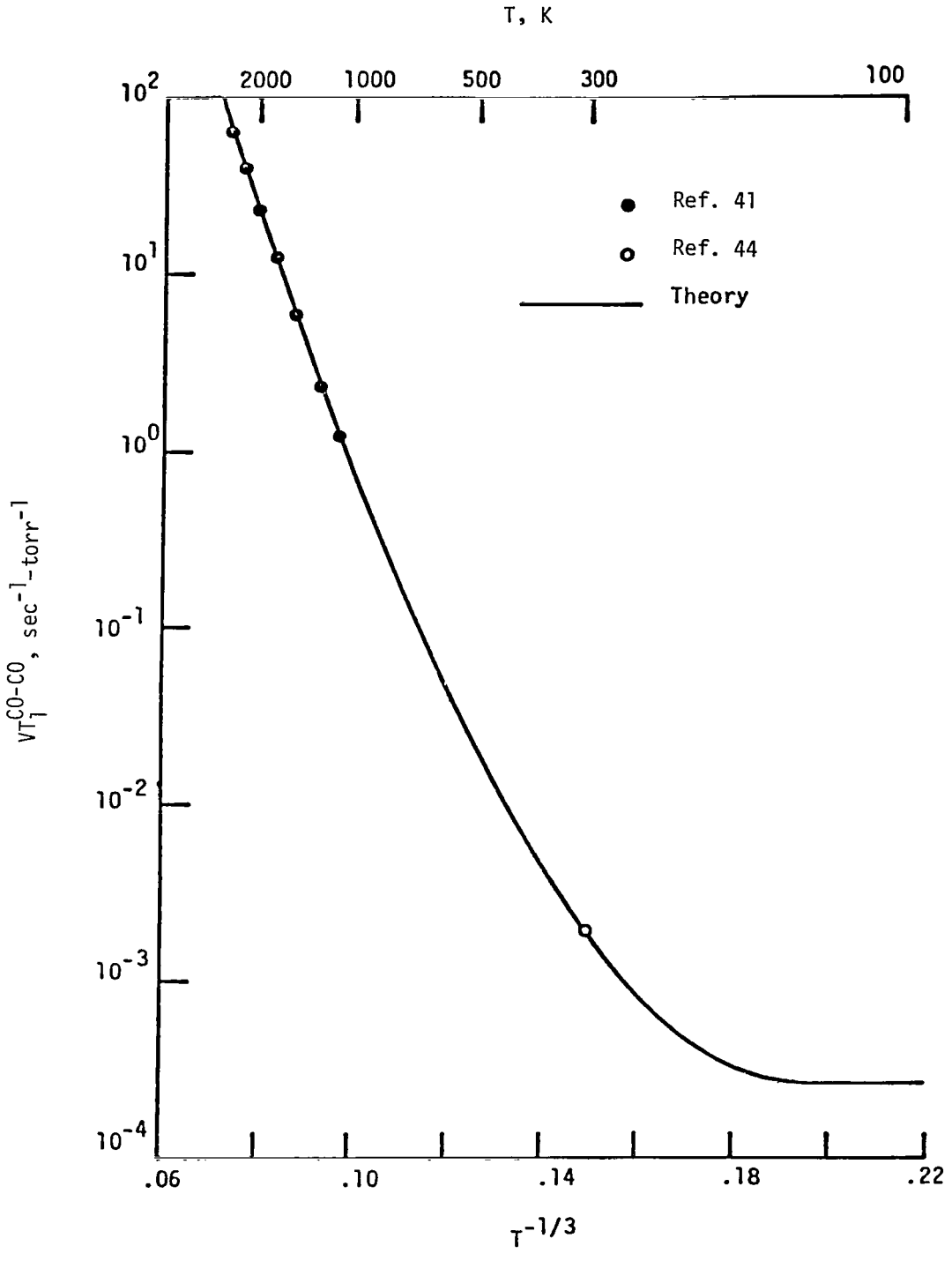

Figure 10.- V-T rate coefficient for deactivation of CO (v = 1) by CO.

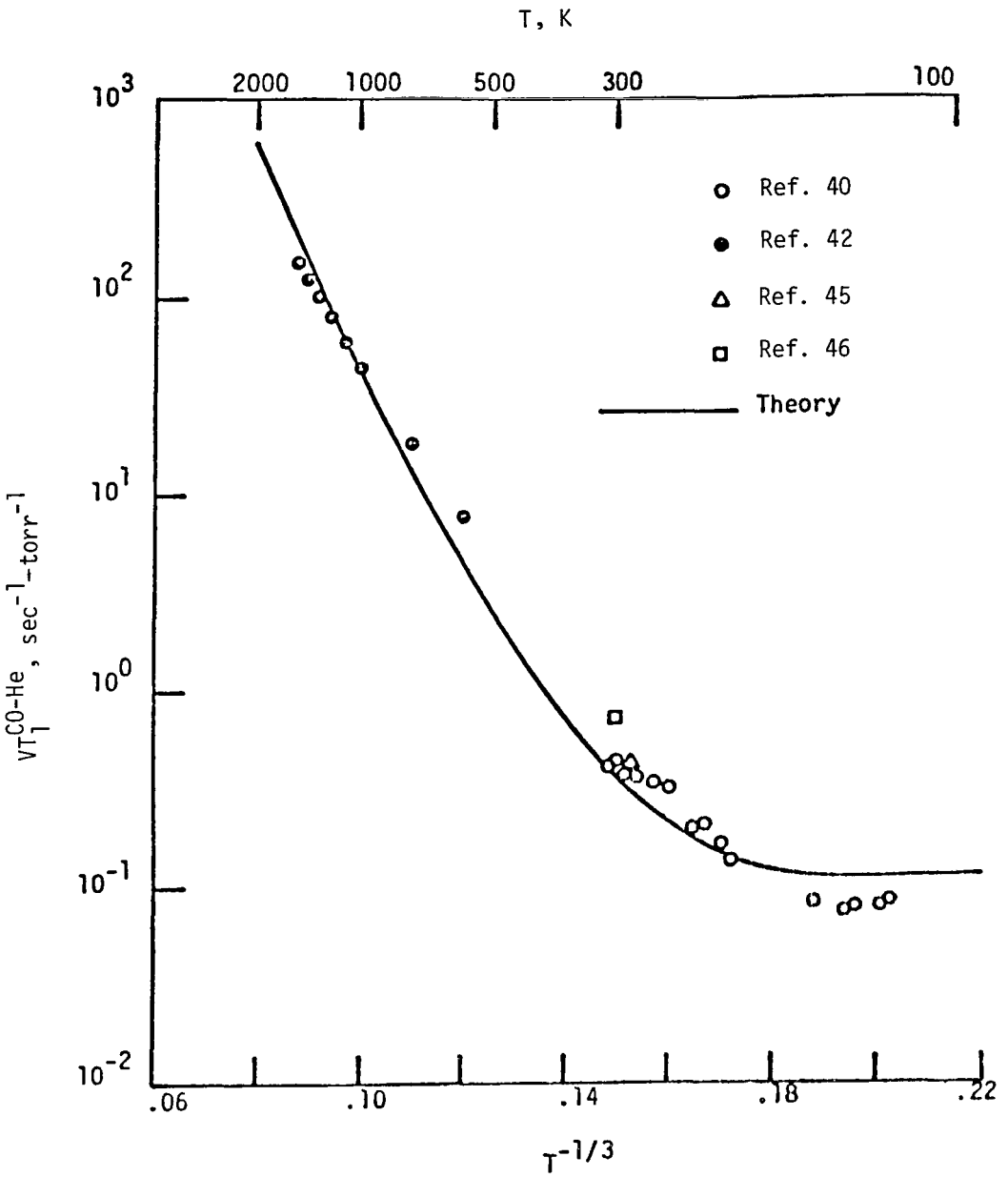

Figure 11.- V-T rate coefficient for deactivation of CO (v = 1) by He.

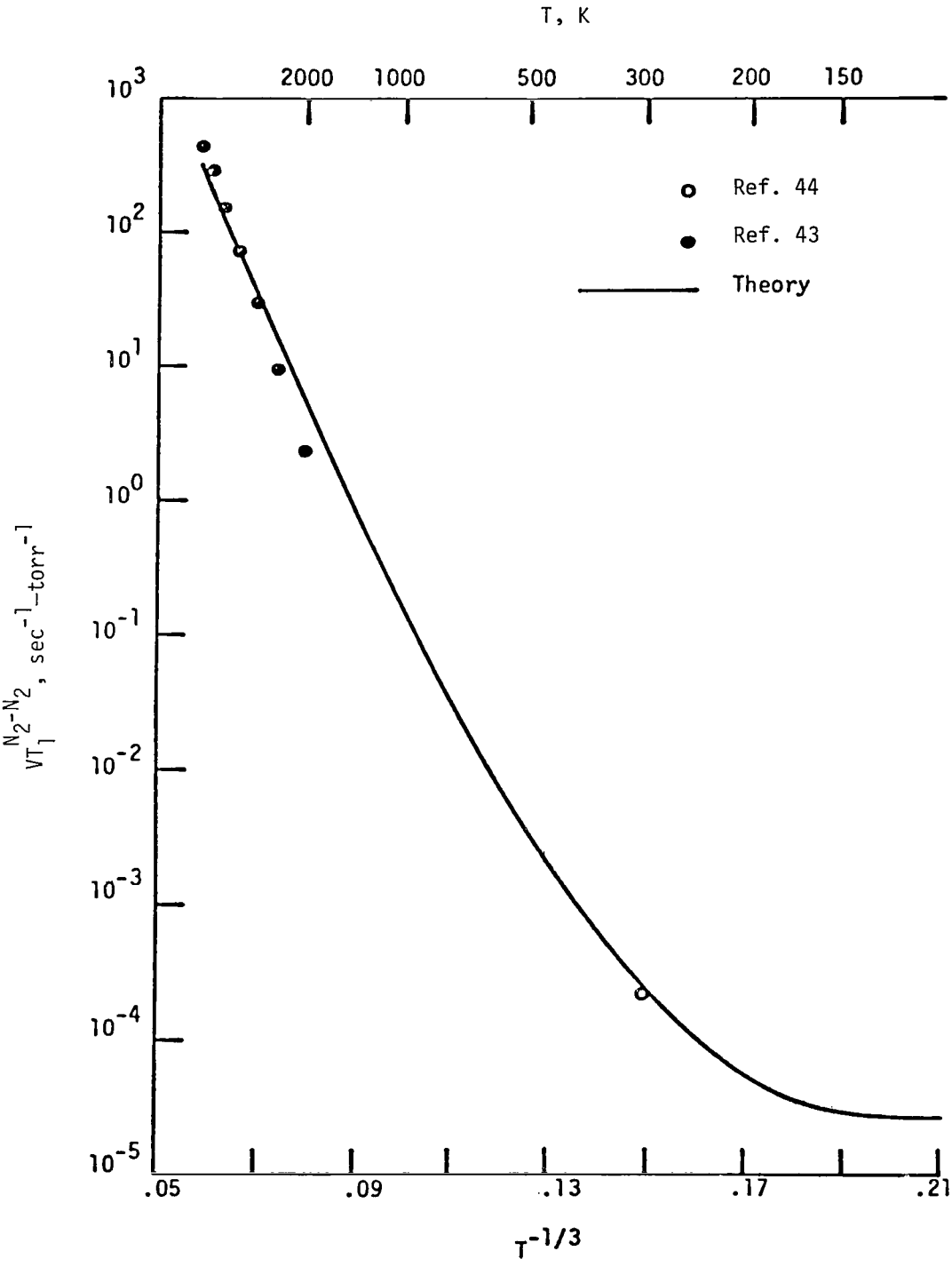

Figure 12.- V-T rate coefficient for deactivation of N_2 (v = 1) by N_2.

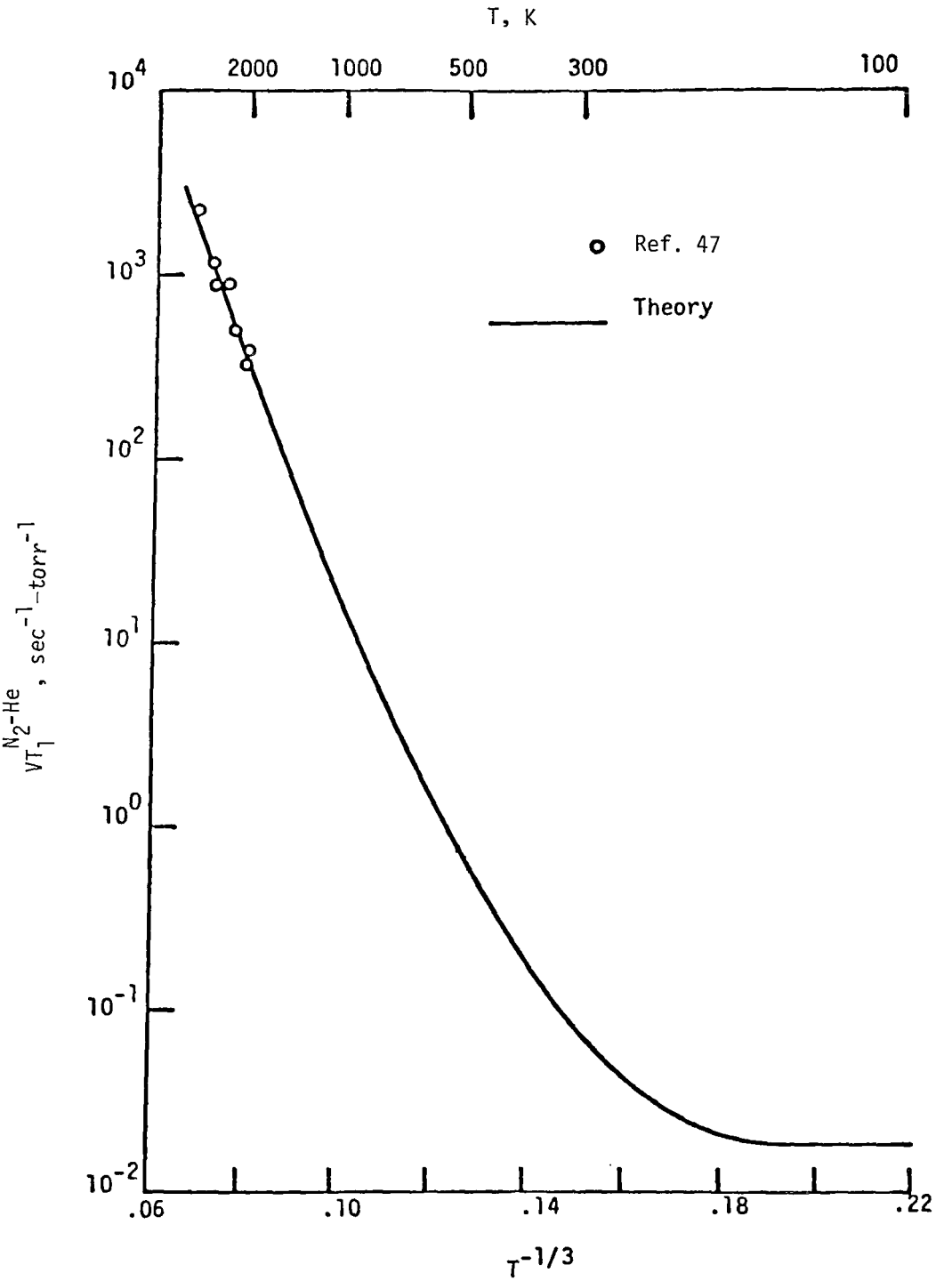

Figure 13.- V-T rate coefficient for deactivation of N_2 (v = 1) by He.

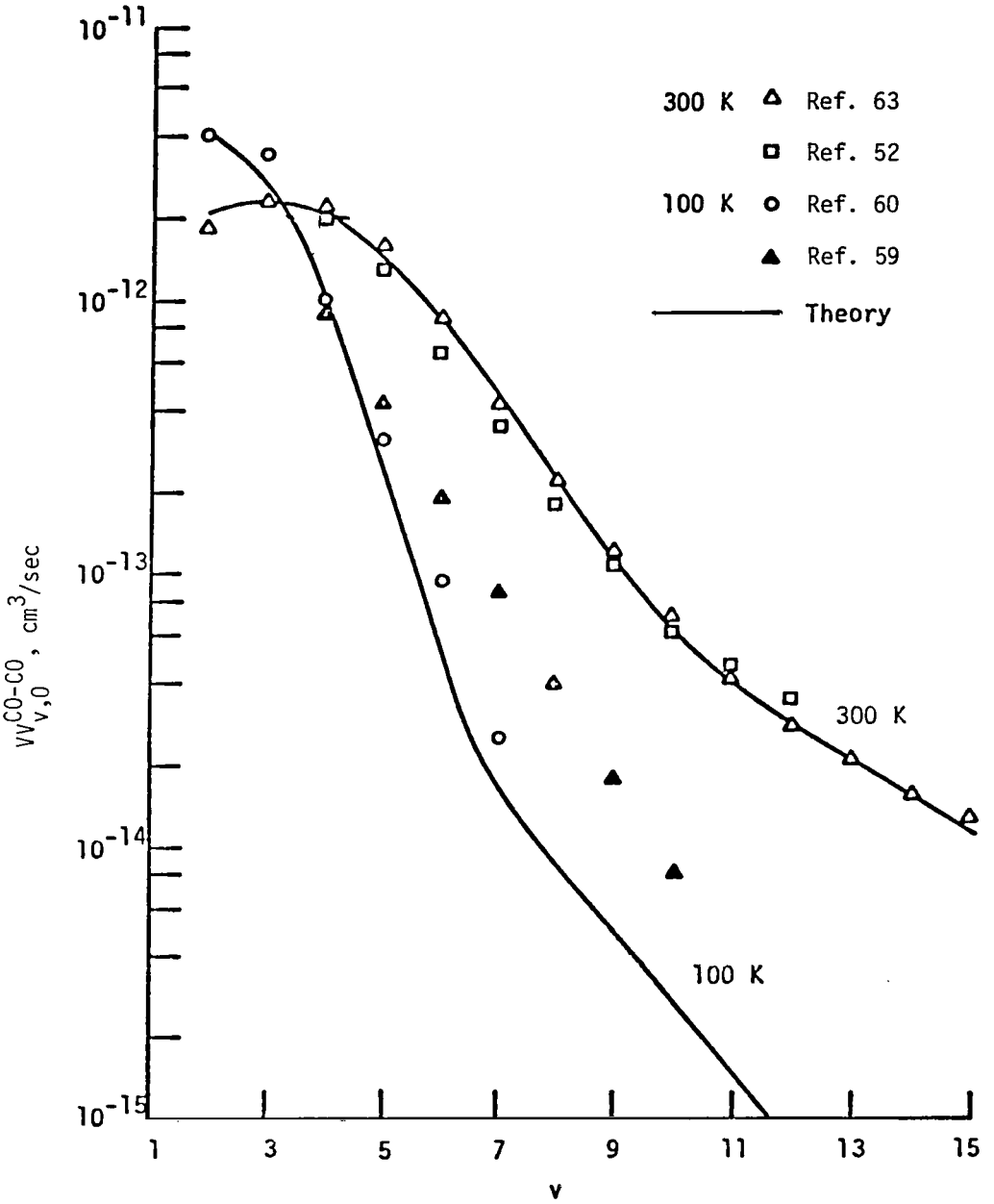

Figure 14.- CO-CO V-V rate coefficients.

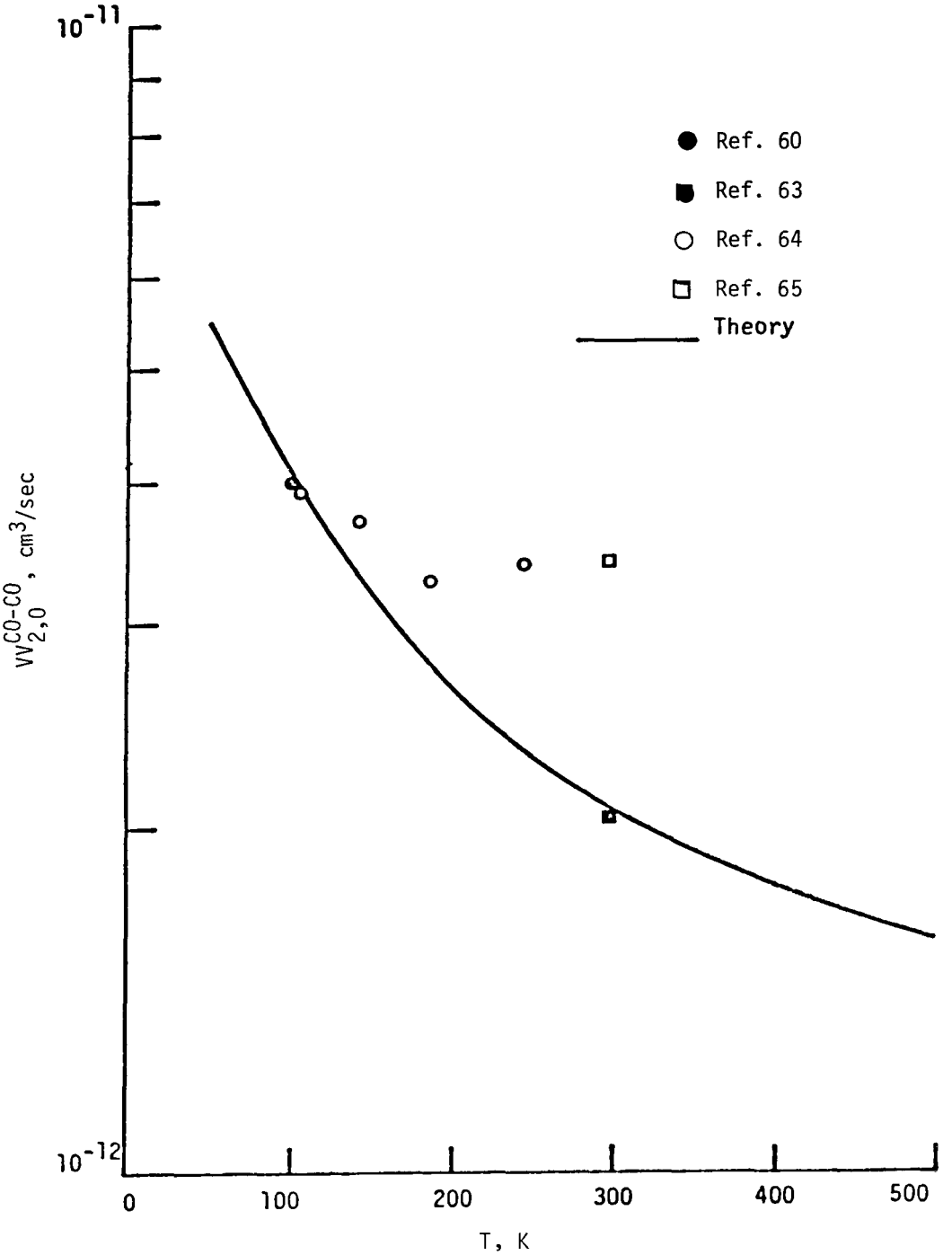

Figure 15.- Temperature dependence of rate coefficient $VV_{2,0}^{CO-CO}$.

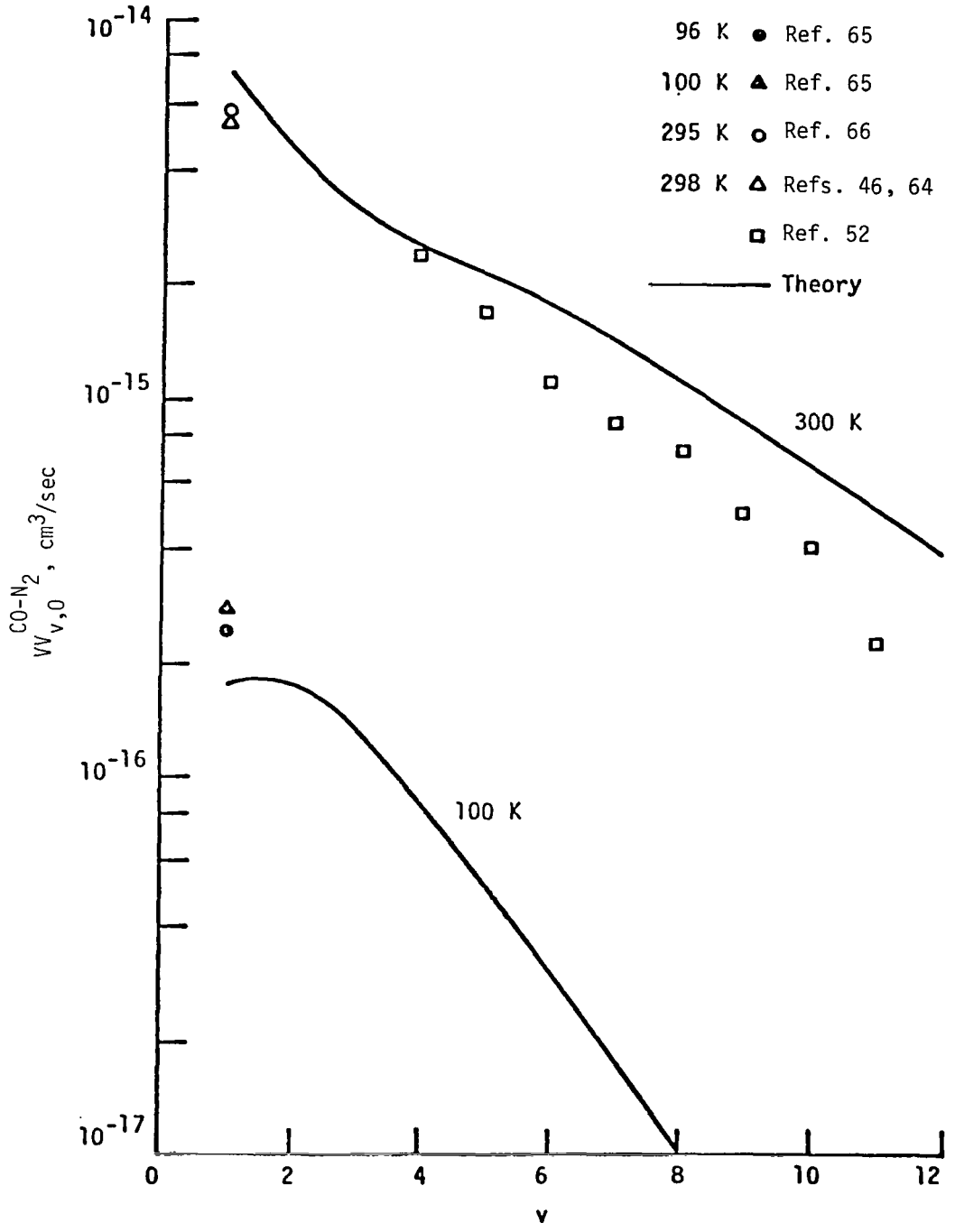

Figure 16.- $CO-N_2$ V-V rate coefficients.

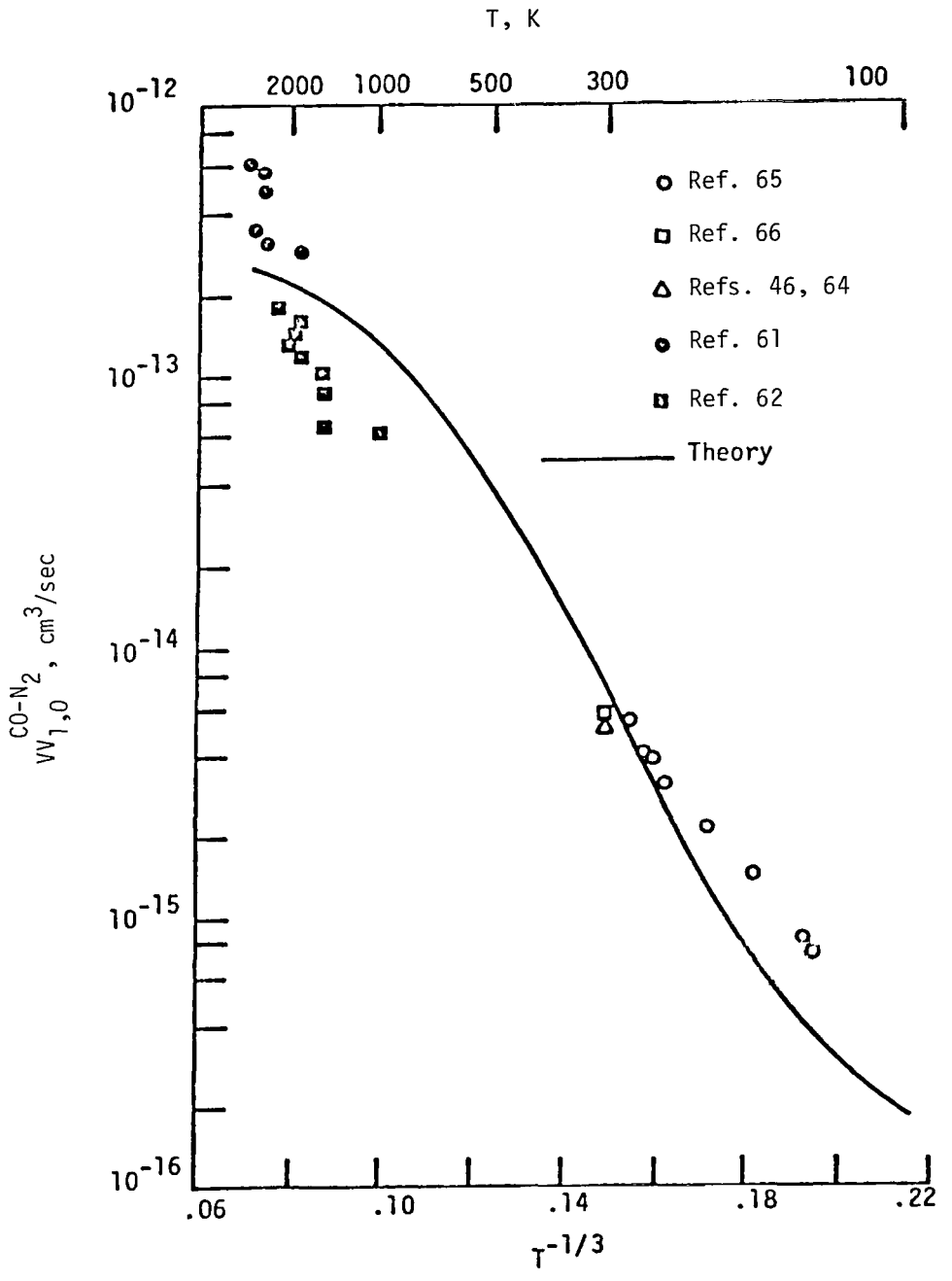

Figure 17.- Temperature dependence of rate coefficient $VV_{1,0}^{CO-N_2}$.

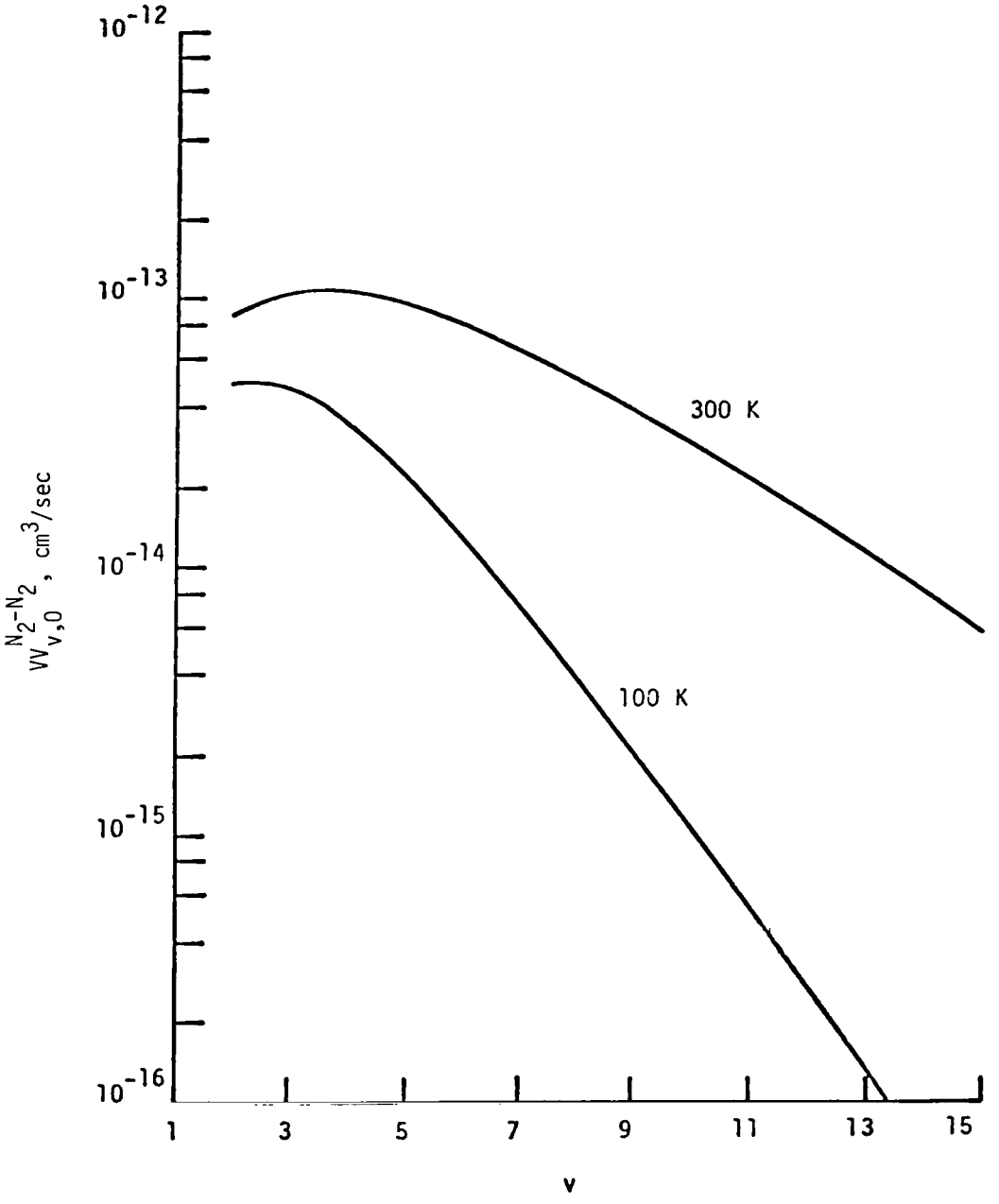

Figure 18.- N_2-N_2 V-V rate coefficients.

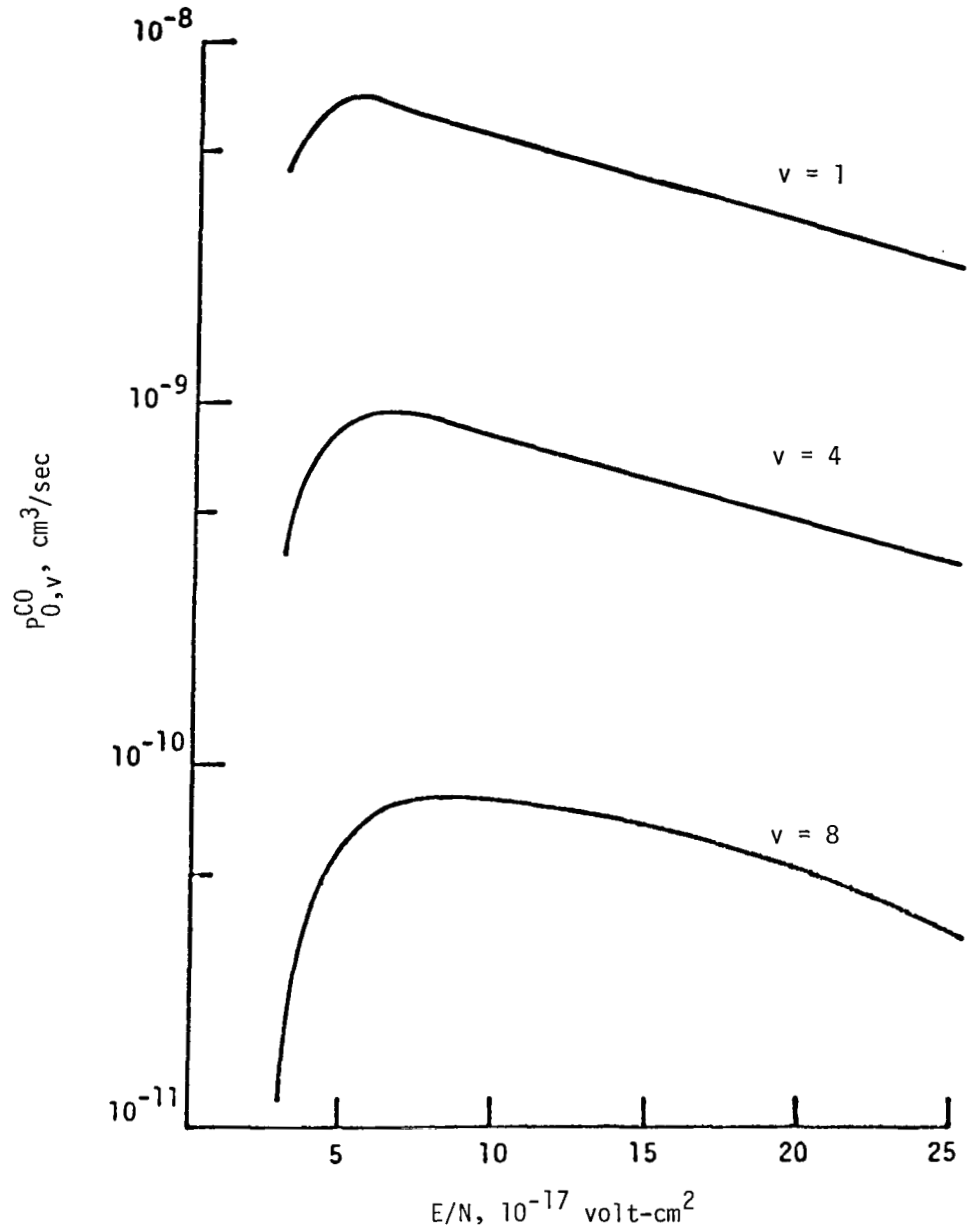

Figure 19.- CO electron vibrational excitation rate coefficients as function of E/N for CO-He mixture of case 1.

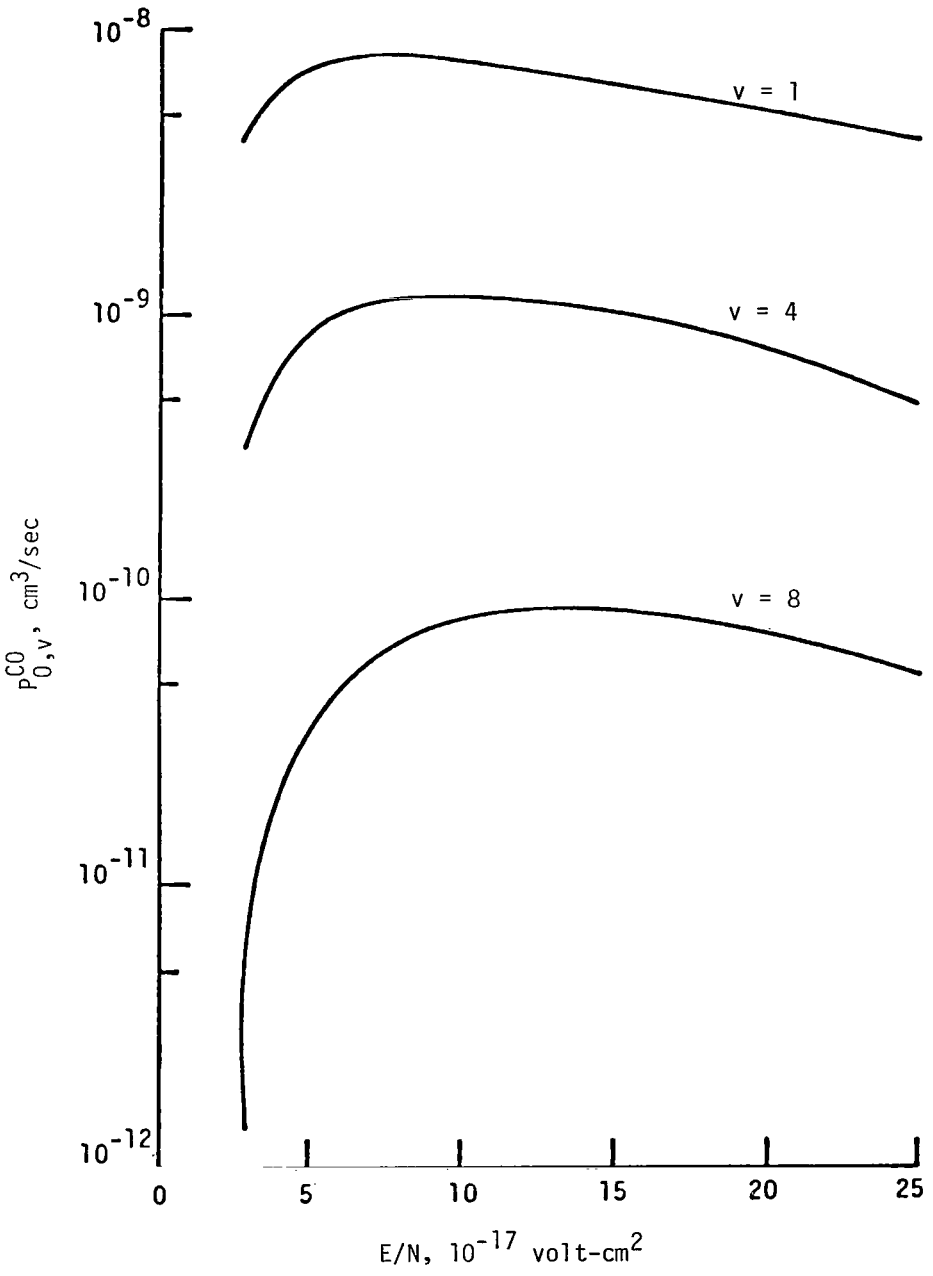

Figure 20.- CO electron vibrational excitation rate coefficients as function of E/N for CO-N_2-He mixture of case 4.

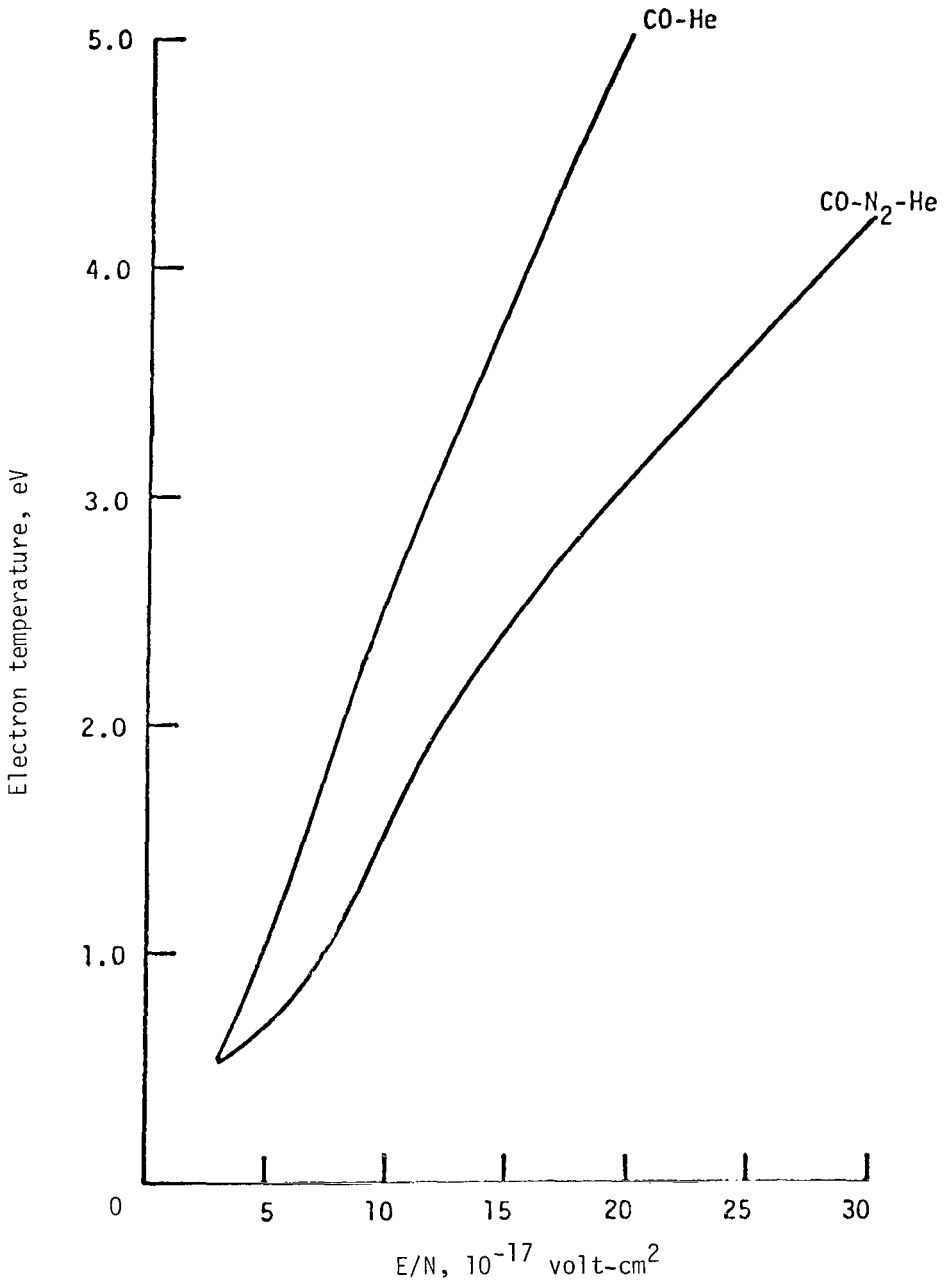

Figure 21.- Electron temperature as function of E/N for CO-He mixture of case 1 and CO-N_2-He mixture of case 4.

NATIONAL AERONAUTICS AND SPACE ADMINISTRATION
WASHINGTON, D.C. 20546

OFFICIAL BUSINESS
PENALTY FOR PRIVATE USE $300

SPECIAL FOURTH-CLASS RATE
BOOK

POSTAGE AND FEES PAID
NATIONAL AERONAUTICS AND
SPACE ADMINISTRATION
451

U.S.MAIL

470 001 C1 U D 760416 S00903DS
DEPT OF THE AIR FORCE
AF WEAPONS LABORATORY
ATTN: TECHNICAL LIBRARY (SUL)
KIRTLAND AFB NM 87117

POSTMASTER: If Undeliverable (Section 158 Postal Manual) Do Not Return

"The aeronautical and space activities of the United States shall be conducted so as to contribute . . . to the expansion of human knowledge of phenomena in the atmosphere and space. The Administration shall provide for the widest practicable and appropriate dissemination of information concerning its activities and the results thereof."

—NATIONAL AERONAUTICS AND SPACE ACT OF 1958

NASA SCIENTIFIC AND TECHNICAL PUBLICATIONS

TECHNICAL REPORTS: Scientific and technical information considered important, complete, and a lasting contribution to existing knowledge.

TECHNICAL NOTES: Information less broad in scope but nevertheless of importance as a contribution to existing knowledge.

TECHNICAL MEMORANDUMS: Information receiving limited distribution because of preliminary data, security classification, or other reasons. Also includes conference proceedings with either limited or unlimited distribution.

CONTRACTOR REPORTS: Scientific and technical information generated under a NASA contract or grant and considered an important contribution to existing knowledge.

TECHNICAL TRANSLATIONS: Information published in a foreign language considered to merit NASA distribution in English.

SPECIAL PUBLICATIONS: Information derived from or of value to NASA activities. Publications include final reports of major projects, monographs, data compilations, handbooks, sourcebooks, and special bibliographies.

TECHNOLOGY UTILIZATION PUBLICATIONS: Information on technology used by NASA that may be of particular interest in commercial and other non-aerospace applications. Publications include Tech Briefs, Technology Utilization Reports and Technology Surveys.

Details on the availability of these publications may be obtained from:

SCIENTIFIC AND TECHNICAL INFORMATION OFFICE

NATIONAL AERONAUTICS AND SPACE ADMINISTRATION

Washington, D.C. 20546